NOAA Technical Memorandum NMFS-AFSC-437

Summary of Temperature and Depth Recorder Data from the Alaska Fisheries Science Center's Longline Survey (2005–2021)

K. Siwicke

May 2022

U.S. DEPARTMENT OF COMMERCE

National Oceanic and Atmospheric Administration
National Marine Fisheries Service
Alaska Fisheries Science Center

The National Marine Fisheries Service's Alaska Fisheries Science Center uses the NOAA Technical Memorandum series to issue informal scientific and technical publications when complete formal review and editorial processing are not appropriate or feasible. Documents within this series reflect sound professional work and may be referenced in the formal scientific and technical literature.

The NMFS-AFSC Technical Memorandum series of the Alaska Fisheries Science Center continues the NMFS-F/NWC series established in 1970 by the Northwest Fisheries Center. The NMFS-NWFSC series is currently used by the Northwest Fisheries Science Center.

This document should be cited as follows:

Siwicke, K. 2022. Summary of temperature and depth recorder data from the Alaska Fisheries Science Center's longline survey (2005–2021). U.S. Dep. Commer., NOAA Tech. Memo. NMFS-AFSC-437, 74 p.

This document is available online at:

Document available: https://repository.library.noaa.gov

Summary of Temperature and Depth Recorder Data from the Alaska Fisheries Science Center's Longline Survey (2005–2021)

K. Siwicke

Auke Bay Laboratories
Alaska Fisheries Science Center
National Marine Fisheries Service
17109 Lena Point Loop Road
Juneau, AK 99801

U.S. DEPARTMENT OF COMMERCE

National Oceanic and Atmospheric Administration
National Marine Fisheries Service
Alaska Fisheries Science Center

NOAA Technical Memorandum NOAA-TM-AFSC-437

May 2022

ABSTRACT

The Alaska Fisheries Science Center (AFSC) longline survey has attached a temperature and depth recorder (TDR) to the fishing gear since 2005 to provide in situ bottom temperature observations. A standardized method for assigning bottom temperature and depth and processing temperature-depth profiles for each station from the TDR was established, with quality assurance and control steps documented. This information is summarized across regions and years. Several potential uses of this dataset are explored: 1) contribution of subsurface temperature time-series to ecosystem indicator syntheses, 2) assignment of temperature to survey catch by depth, 3) characterization of temperature inversion layers, 4) identification of tidal fluctuations during survey sets, and 5) assessment of potential bias in depth observations recorded during the AFSC longline survey. These analyses provide the background and context for monitoring water temperatures at depth along the continental shelf-break/slope of the Gulf of Alaska, Bering Sea, and Aleutian Islands, particularly as they relate to the AFSC longline survey and groundfish.

CONTENTS

INTRODUCTION

The water temperature of the surface layer of the ocean has increased over the last century (Meehl et al. 2016), and this heat can be transferred to the deep ocean via mixing (e.g., wind and waves) and stored for millennia (Nieves et al. 2015). Fisheries across the globe are already showing signs of warming temperatures influencing catch (Cheung et al. 2013). Temperature can limit distributions of species distributions (Stevenson and Lauth 2019, Meuter and Litzow 2008), impact biological processes such as growth rates (Krieger et al. 2020), or influence available spawning habitat (Laurel et al. 2020). To understand how changes in the physical environment influence fisheries resources, it is important to monitor temperature at depth during fisheries surveys.

NOAA's Alaska Fisheries Science Center (AFSC) conducts several fisheries surveys to provide fishery-independent information for stock assessments, in addition to environmental data such as subsurface temperature. The AFSC conducts various bottom-trawl surveys in Alaska, and all have a long history of collecting bottom temperature, such as the eastern Bering Sea survey which began temperature collections in 1982 (Buckley et al. 2009). This temperature data has been used to monitor the extent and effect of the cold pool (Kotwicki and Lauth 2013, Thorson 2019) and validate a regional ocean model (Kearney et al. 2020). The AFSC has been conducting a longline survey since 1987 to sample groundfish from the upper continental slope annually in the Gulf of Alaska (GOA), during odd years in the Bering Sea (BS), and during even years in the Aleutian Islands (AI). Beginning in 2005, a temperature and depth recorder (TDR) has been used for the purpose of measuring in situ bottom temperature at each station. These data have not been formally processed or reported in annual cruise reports, but a single bottom temperature for stations has been uploaded to the Alaska Fisheries Network (AKFIN) and available to authorized users.

The design and execution of the AFSC bottom trawl surveys differs a great deal from the AFSC longline survey, and thus methods for analyzing data from the former are not easily adapted to the latter. Because the TDR is attached to the headrope of the trawl net and covers a swath above the seafloor (usually with little bathymetric relief), it provides a temperature that is derived from measurements along the track line that is fished (approximately 30 minutes), and the mean of the temperature recorded provides a good measurement of the near-bottom temperature related to the entire trawl catch (Lauth et al. 2019). In contrast, the TDR attached to the longline is only measuring a localized point on the seafloor while a typical AFSC longline survey set samples catch over its 16 to 18 km length, which soaks for several hours, and occurs over depth changes of hundreds of meters. Therefore, the mean bottom temperature is really only representative of the thermal environment experienced by fish caught near the TDR. Standardized methods for processing, reporting, and analyzing the AFSC longline survey's temperature data are established herein, so this subsurface temperature data can be more broadly understood and utilized.

The objective of this Technical Memorandum is to layout the protocols for processing, reporting, and analyzing temperature and depth data recorded by the AFSC longline survey and provide a summary of this information to date. Temperature data analysis and interpretation were separated into two components: temperature-depth profiles captured during the setting of gear (downcast) and bottom temperatures recorded during fishing. Potential uses of TDR data from the AFSC longline survey are explored including 1) an ecosystem status report contribution to syntheses related to Alaska's subsurface temperature environment, 2) assigning temperature to depth-specific catch, 3) characterizing temperature inversion layers, 4) identifying when high and low tides are occurring during survey sets, and 5) assessing bias in the method for recording depths during the survey.

LONGLINE SURVEY TEMPERATURE AND DEPTH ANALYSIS

Data Collection

The AFSC's annual longline survey begins each year in late May and concludes in late August, systematically sampling approximately 85 stations annually. Most sampling stations consist of two sets of gear laid end to end, and each set is comprised of 80 or 90 units or "skates" of gear, where one skate of gear contains 45 hooks. The AFSC longline survey is depth stratified, and the strata used in the survey and stock assessments are < 100 m, 101–200 m, 201–300 m, 301–400 m, 401–600 m, 601–800 m, 801–1,000 m, and 1,001–1,200 m. As skates reach the vessel rail, contracted fisheries biologists record the depth from the depth-finder (i.e., sonar) at the first/last skate, every fifth skate, and skates at which the depth stratum changes. A linear interpolation is used to assign depths for skates that were not directly observed, resulting in catch from every skate being associated with a depth, while fish length data are associated only with a depth stratum. Following geographical distinctions used by the AFSC longline survey, we aggregated data into the following five regions: eastern Gulf of Alaska (EGOA), central Gulf of Alaska (CGOA), western Gulf of Alaska (WGOA), AI (only sampled even years), and BS (only sampled odd years) (Fig. 1). Note that the standard survey stations are sampled during six legs, beginning with the BS or AI depending on the year, then sampling west to east in the WGOA to station 75 before transiting to the furthest southeast station (148) and sampling from east to west and ending at station 121 (Fig. 1). Further details on the AFSC longline survey can be found in annual cruise reports (e.g., Siwicke et al. 2022), and specific protocols can be found at: https://www.fisheries.noaa.gov/resource/document/survey-protocol-alaska-sablefish-longline-survey.

A TDR has been attached to the first set of fishing gear to measure the water temperature at the bottom since 2005. The TDR used on the AFSC longline survey is an SBE39 (Sea-Bird Scientific) with a titanium housing and depth rating to 2,000+ meters. These units are further housed in a PVC tube that is enclosed on the top, open to the water on the end with the temperature sensor (with a stainless steel bolt fastened through the middle to retain the unit), and attached to the spliced loop between skates via a stainless steel locking carabineer and eyelet through the top of the PVC tube. Date/time, pressure (converted to depth in meters), and temperature (°C) were recorded every 10 seconds. Following training, contracted fisheries biologists on the AFSC longline survey have been responsible for initializing the instrument before setting, providing it to the fishing crew for deployment, and downloading the data following retrieval using Sea-Bird Scientific's SeaTerm software. The vessel captain records station data on a haul form that the contract biologists enter into the at-sea database, which includes (starting in 2020) the latitude and longitude at which the TDR is deployed (Fig. 2). No temperature-depth profile information has previously been processed, and reanalysis of this data strived for accuracy and consistency.

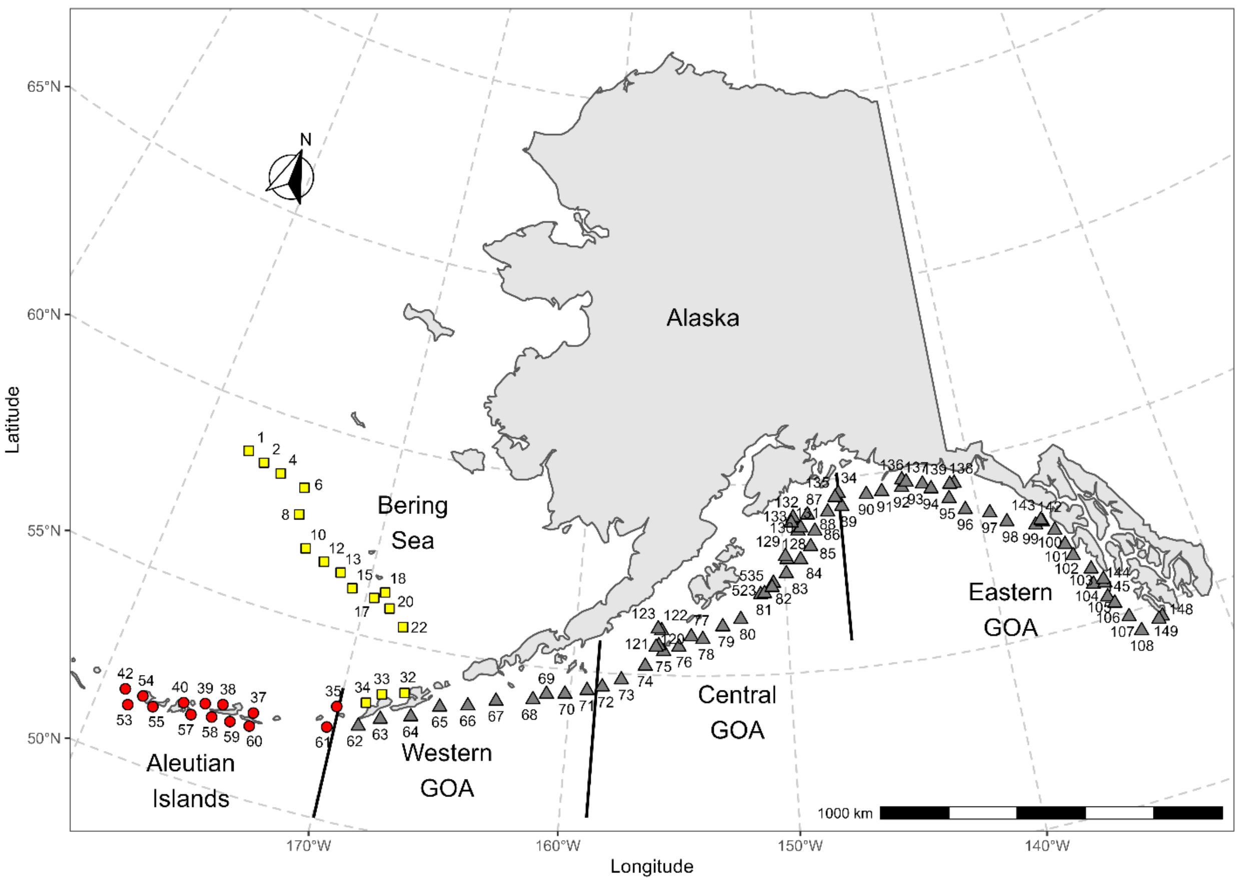

Figure 1. -- Map of the Alaska Fisheries Science Center's longline survey stations and management regions. Dark triangles indicate annual sampling, while yellow squares are sampled in odd years and red circles are sampled in even years.

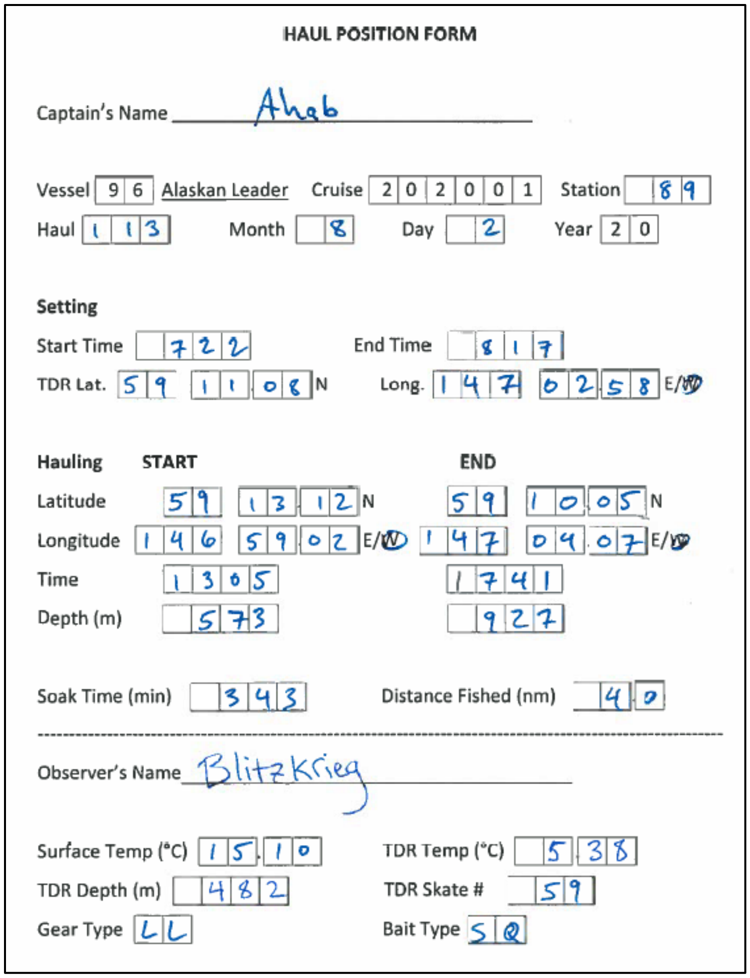

HAUL POSITION FORM

Captain's Name Ahab

Vessel 96 Alaskan Leader Cruise 202001 Station 89

Haul 113 Month 8 Day 2 Year 20

Setting

Start Time 722 End Time 817

TDR Lat. 59 11.08 N Long. 147 02.58 E/W

Hauling	START	END
Latitude	59 13.12 N	59 10.05 N
Longitude	146 59.02 E/W	147 04.07 E/W
Time	1305	1741
Depth (m)	573	927

Soak Time (min) 343 Distance Fished (nm) 4.0

Observer's Name Blitzkrieg

Surface Temp (°C) 15.10 TDR Temp (°C) 5.38

TDR Depth (m) 482 TDR Skate # 59

Gear Type LL Bait Type SQ

Figure 2. -- Haul position form (2020 version) which includes the latitude and longitude where the TDR was deployed and the skate on which it was retrieved.

Data Processing

Temperature and depth data from all years were reprocessed in a consistent manner. Data from the TDR can be broken into three parts: 1) a temperature-depth profile during the setting of gear (downcast), 2) a bottom depth and temperature while the gear is fishing, and 3) a temperature-depth profile during the retrieval of gear (upcast). The downcast/upcast is filtered to remove data when the unit is on deck (i.e., depth < 0 m) and when the gear was descending/ascending too slowly (change in depth < 1.2 m in 10-sec interval). Without the latter filter, interpolation to 1-m intervals includes more spurious values. Mean bottom depth and water temperature were determined from records while the TDR was stationary (i.e., little to no movement) on the bottom; data was cleaned by first filtering by change in depth ≤ 0.03 m vertically in 10-sec intervals and within 30 m of the maximum bottom depth, and then further narrowed down to within ± 5 m of the mean. Disturbances to the TDR, such as gear being dragged deeper during haul back, occasionally disrupt this algorithm, and in those cases, disturbed data were manually removed before running the script. The minimum and maximum bottom water temperature were also determined as a metric for variability experienced while on the bottom. Because the TDR can occasionally accumulate mud on the temperature sensor during retrieval, the upcast temperature data were discarded, but the timestamp at the top of the upcast was utilized for estimating which skate the TDR was retrieved from.

After the biologists download the data in SeaTerm, two quality assurance/quality control (QAQC) R-scripts are used to parse the data as outlined above and produce three graphical representations. Before 2019, occasional transcription errors in depths and locations were not being detected, so visual checks for at-sea corrections were implemented. The first script produces a graphic of the depth and temperature data recorded by the TDR (Fig. 3).The second script incorporates the depths (recorded and interpolated) of each skate and the start/end points to produce a depth profile of the station from data in the at-sea database (Fig. 4). Finally, a map of expected and realized latitudes and longitudes is used to confirm the start and end positions are reasonable (Fig. 5). Combined, these graphics provide a quick and easy way to identify errors in depths and positions from transcription errors while at sea, and corrections are made prior to the data reaching the final database. The gear depth and temperature are included in the haul information that goes into the AFSC Longline Survey Database and is subsequently available via the Alaska Fisheries Information Network (AKFIN, https://akfin.psmfc.org/).

Post-survey processing of temperature profiles is done to repackage this data so that it is consistent across stations and years. Note that profile data have not historically been post-processed. The raw temperature profile was interpolated to 1-m increments via the double parabolic method used by the World Ocean Atlas 2018 (Reiniger and Ross 1968, Locarnini et al. 2019). This data can also be binned to the depth stratum level, though caution is necessary when a stratum is only partially sampled. A user can additionally define their own post-processed product as desired, as this 1-m increment data can easily be binned into layers that are flexible depending on the scale a user is interested in.

The skate at which the TDR was attached was not explicitly recorded until 2020, and thus, it was inferred from the data to estimate the geographic coordinates of the deployment. The crew sets gear by tub, equal to two skates, and the TDR is typically attached at tub 30 which is skate 59 (i.e., this is what was specified in the survey operations plan), with the exception of 2017, when it appears that it was attached at tub 35 (skate 69). It is possible for the TDR to be set on a different nearby skate or for gear to part and have to be retrieved in a reverse order, such that it is not assumed that the TDR is always associated with the intended skate number recorded by the biologist and input to the database. For an initial estimate of which skate the TDR was attached to, the timestamp at the top of the TDR's upcast, when it broke the surface of the water, was matched to the nearest skate using the biologist recorded timestamps at each skate. Diagnostic plots were used to assess how well the TDR recorded bottom depth matched the biologist derived depths of the set. When questionable estimates were encountered, such as an estimated skate number more than five away from expected, logbook notes were used to aid in resolving issues. Only six station-year combinations had errors due to out-of-sync times and were corrected, and one was removed because the TDR depth was much deeper than the entire set and the error could not be resolved. Latitude and longitude were estimated by transposing the standardized track line (a straight line is assumed if a standardized track line did not exist) between the recorded beginning and end points of the set (coordinates recorded at retrieval) using the skate number with the TDR to infer the proportion along the track line (first converted to eastings/northings in meters to ensure a uniform scale) at which the temperature-depth profile and bottom temperature/depth came from (Fig. 5). Beginning in 2020, latitude and longitude were recorded when the TDR was set (downcast), and the skate number at which the TDR is retrieved is also documented to aid in any data discrepancies that may arise.

Beginning in 2019, a second TDR was attached to the second set each day. For regular survey stations, the second set is generally the deeper of the two, but some stations are just one set (e.g., gully stations), and historically only the morning station would have a TDR attached. The purpose of the second TDR is to understand how variable sub-surface water temperature is between two nearby sets in the same day and the potential to interpolate a bottom temperature to nearby (within several kilometers) individual skates from temperature-depth profiles. Additionally, if a TDR on the first set fails to operate or is lost, the data from the second TDR can be used in its stead; this results in fewer gaps in the dataset compared to previous years.

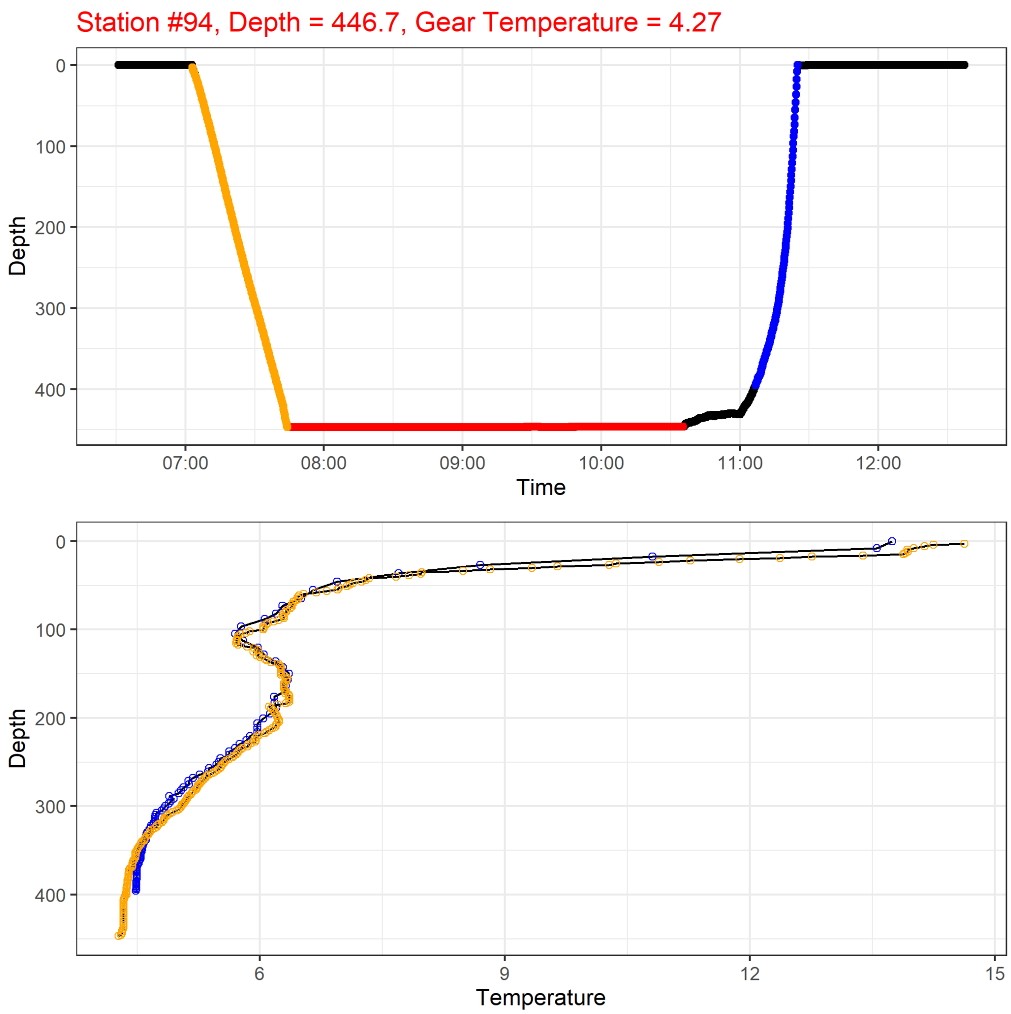

Figure 3. -- An example of the output from the temperature and depth recorder (TDR) at-sea QAQC script. The upper panel shows the depths occupied by the TDR through time with the processed data that was included for the downcast (orange), bottom (red), and upcast (blue). The mean depth and temperature from the bottom are printed at the top and referencing the points highlighted in red; note that black points between the bottom and upcast were filtered out as the haul back begins slowly lifting the TDR off the bottom. The lower panel shows the temperatures recorded on the downcast (orange) and upcast (blue), which correspond to the same colors on the top panel.

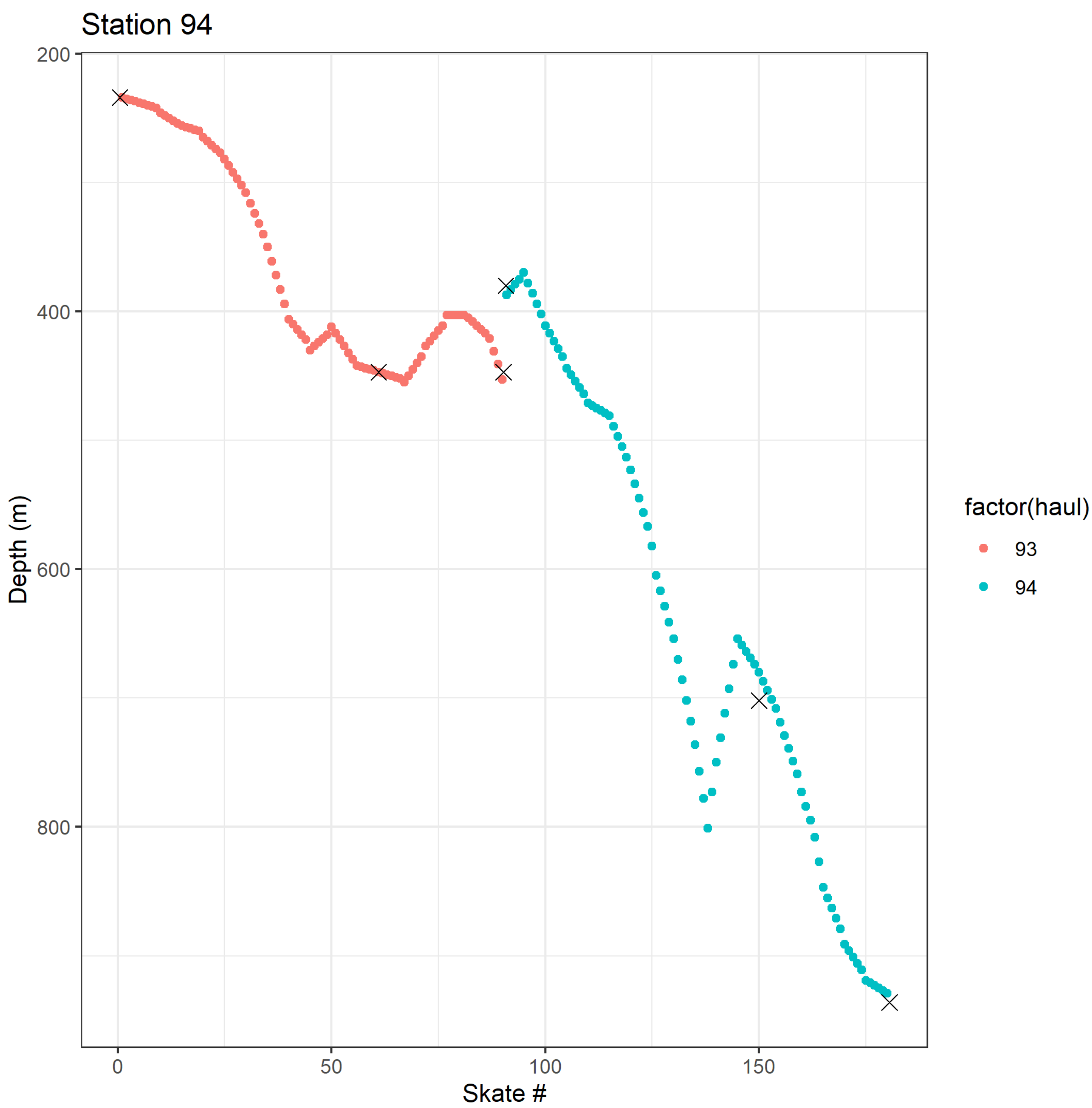

Figure 4. -- An example of at-sea QAQC output from the recorded (and interpolated) depths of each skate from a station (two hauls) where ‘X’ indicate the depth of the start and end of each haul (recorded by the captain on the haul form shown in Fig. 2) in addition to the TDR within each haul.

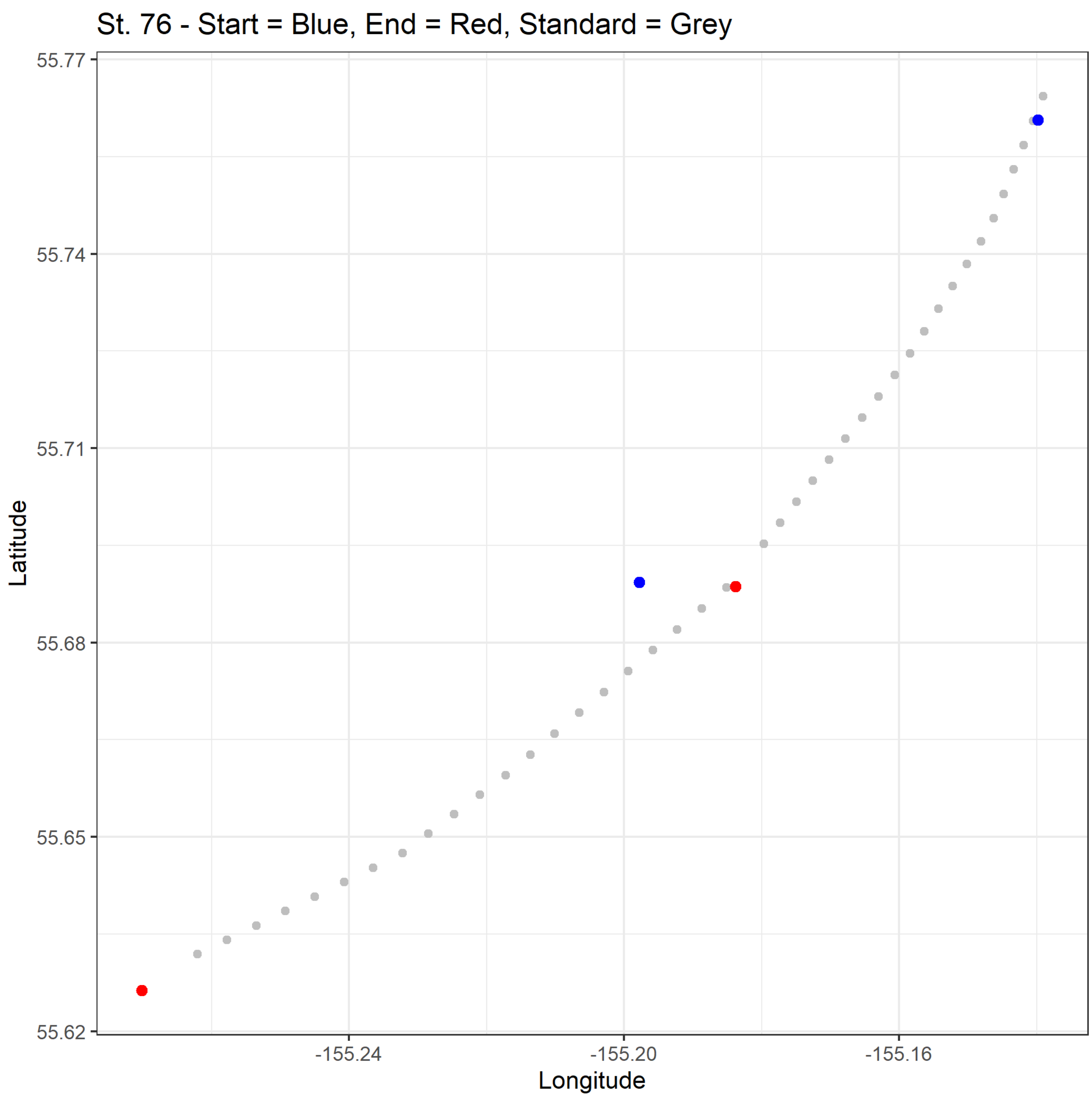

Figure 5. -- An example output from the at-sea QAQC script that shows the target track for the longline sets as grey points and the recorded start (blue points) and end (red points) locations from two hauls at station 76.

Temperature and Depth Summary

Temperature-depth profiles standardized to 1-m increments allow for an easy comparison of subsurface temperature among years, with the surface layer (i.e., the top 10 m) not included. To avoid having a large temperature gradient that exists when looking at an entire temperature-depth profile, data are compared across discrete depth bins: 11–50 m, 51–100 m, 101–200 m, 201–300 m, 301–400 m, and 400+ m. Data have been separated into three groups, BS presented latitudinal, GOA presented longitudinal, and AI presented longitudinal and further separated by north and south of the island chain. The deeper second set TDR data were included when a shallower first set did not exist and was also appended to the shallower cast when it continued deeper than the first set.

Bering Sea

In the BS, there is a general trend of warming from north to south, but overall, relatively warm and cold years are evident in subsurface temperatures. Note that subsurface temperature data in the Bering Sea was not available for 2007 and is thus absent from this summary. In the shallower 11 to 50-m layer, there is a clear cooler period from 2009 through 2013, with similarities in 2005, 2015, 2017, and 2021; the warmest temperatures in the near surface occurred in 2019 (Fig. 6). The same pattern occurs at the 51 to 100-m layer (Fig. 7, note the change in the color scale by each depth range). These cooler periods directly relate to observations from the AFSC bottom trawl survey showing lower than average cold pool extent from 2006 through 2014 (Siddon, 2021), though the station locations are not directly located within the cold pool as they are deeper along the shelf break. As the depth increases, the range of temperature decreases, but the same pattern remains (Figs. 8–11). Inclusion of the second TDR deployment in 2019 and 2021 extends the vertical and horizontal range of temperatures recorded by the AFSC longline survey (Figs. 9–11). When focusing on one subsurface layer (mean of the interpolated 1-m increment temperatures from 246 to 255 m) the north south temperature gradient also is more pronounced during the relatively cooler years, 2009, 2011, and 2013 (Fig. 12).

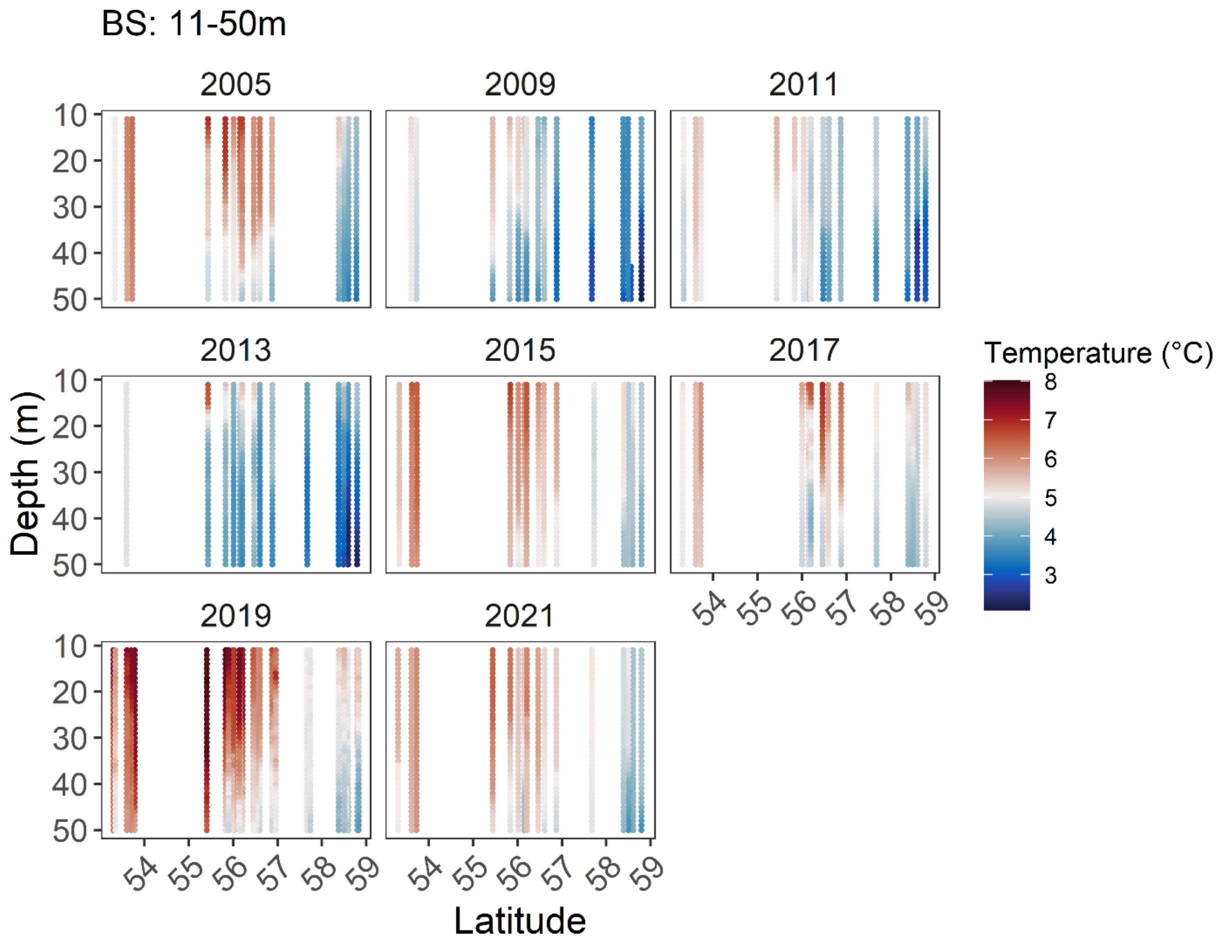

Figure 6. -- Bering Sea temperature (color scale) by year at 1-m increments from depths of 11 to 50 m (y-axis), where the x-axis depicts south to north (left to right).

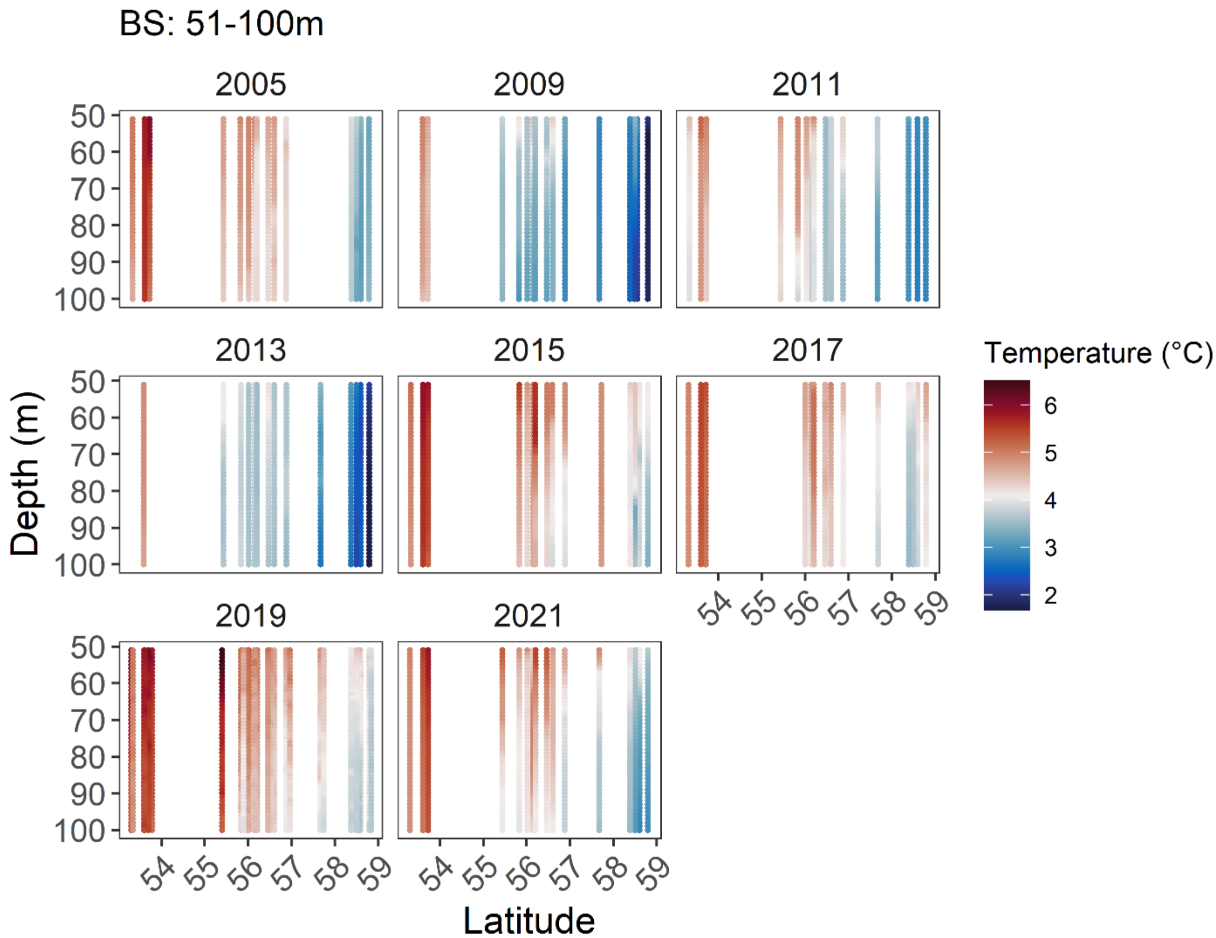

Figure 7. -- Bering Sea temperature (color scale) by year at 1-m increments from depths of 51 to 100 m (y-axis), where the x-axis depicts south to north (left to right).

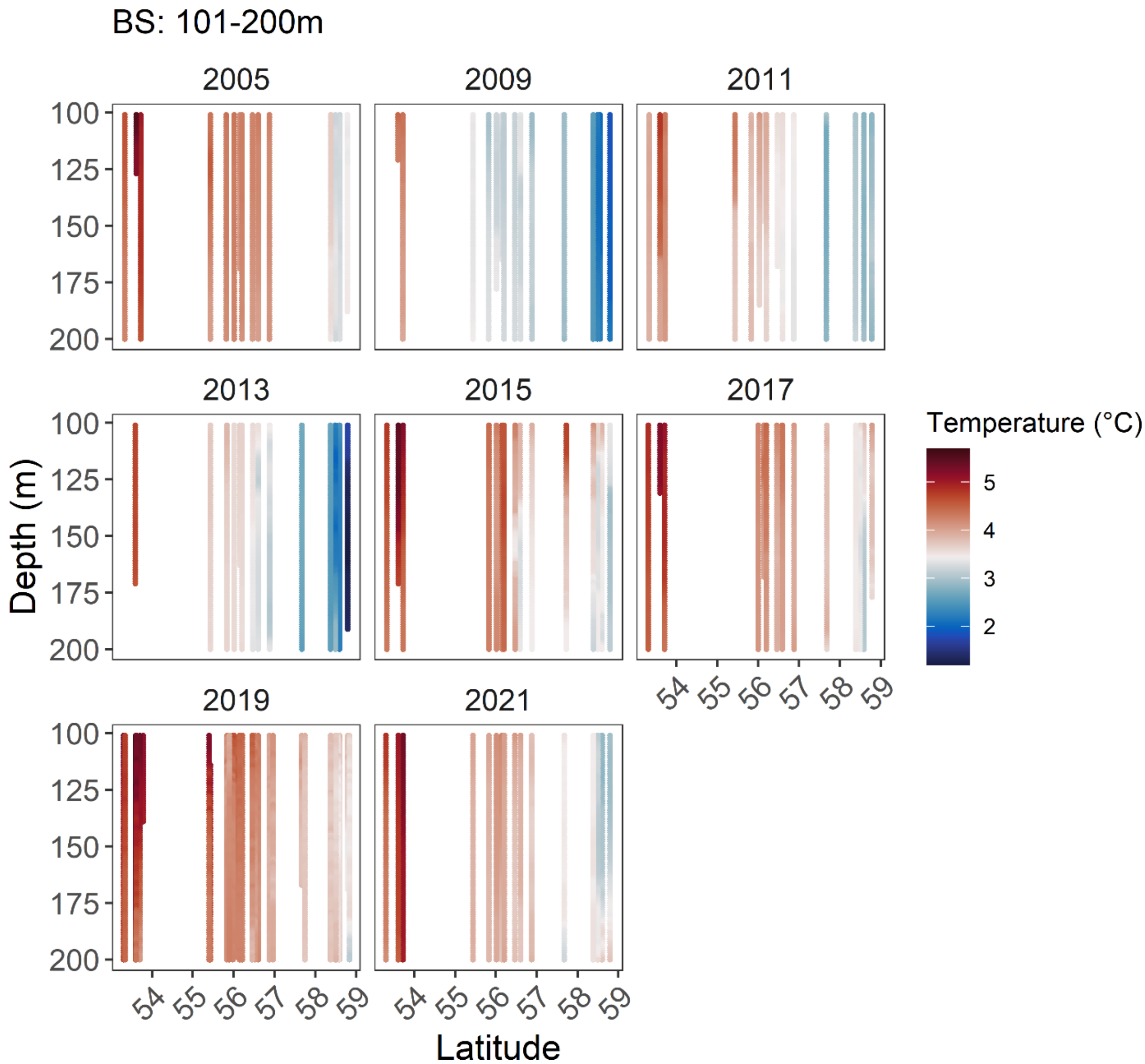

Figure 8. -- Bering Sea temperature (color scale) by year at 1-m increments from depths of 101 to 200 m (y-axis), where the x-axis depicts south to north (left to right).

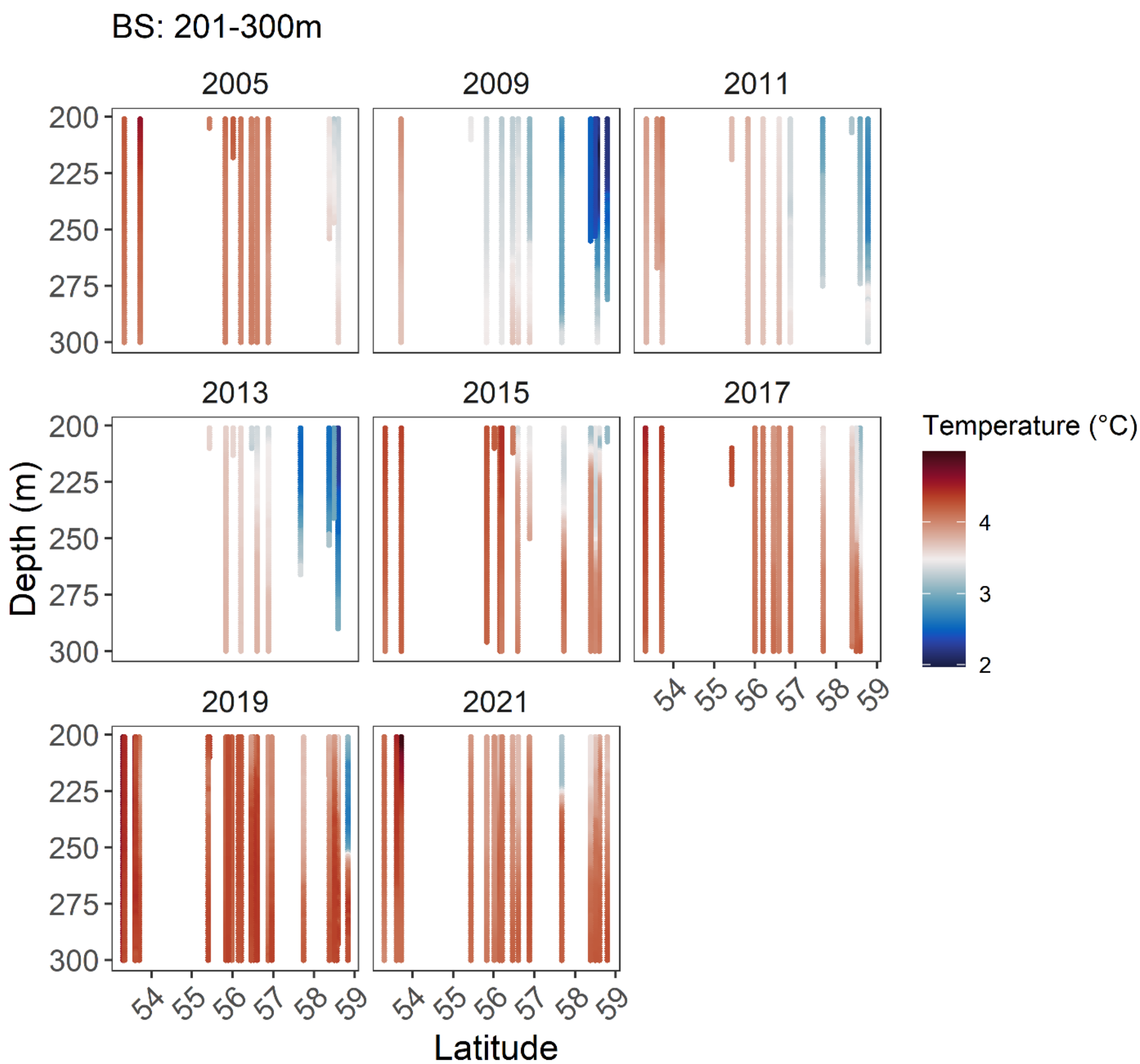

Figure 9. -- Bering Sea temperature (color scale) by year at 1-m increments from depths of 201 to 300 m (y-axis), where the x-axis depicts south to north (left to right).

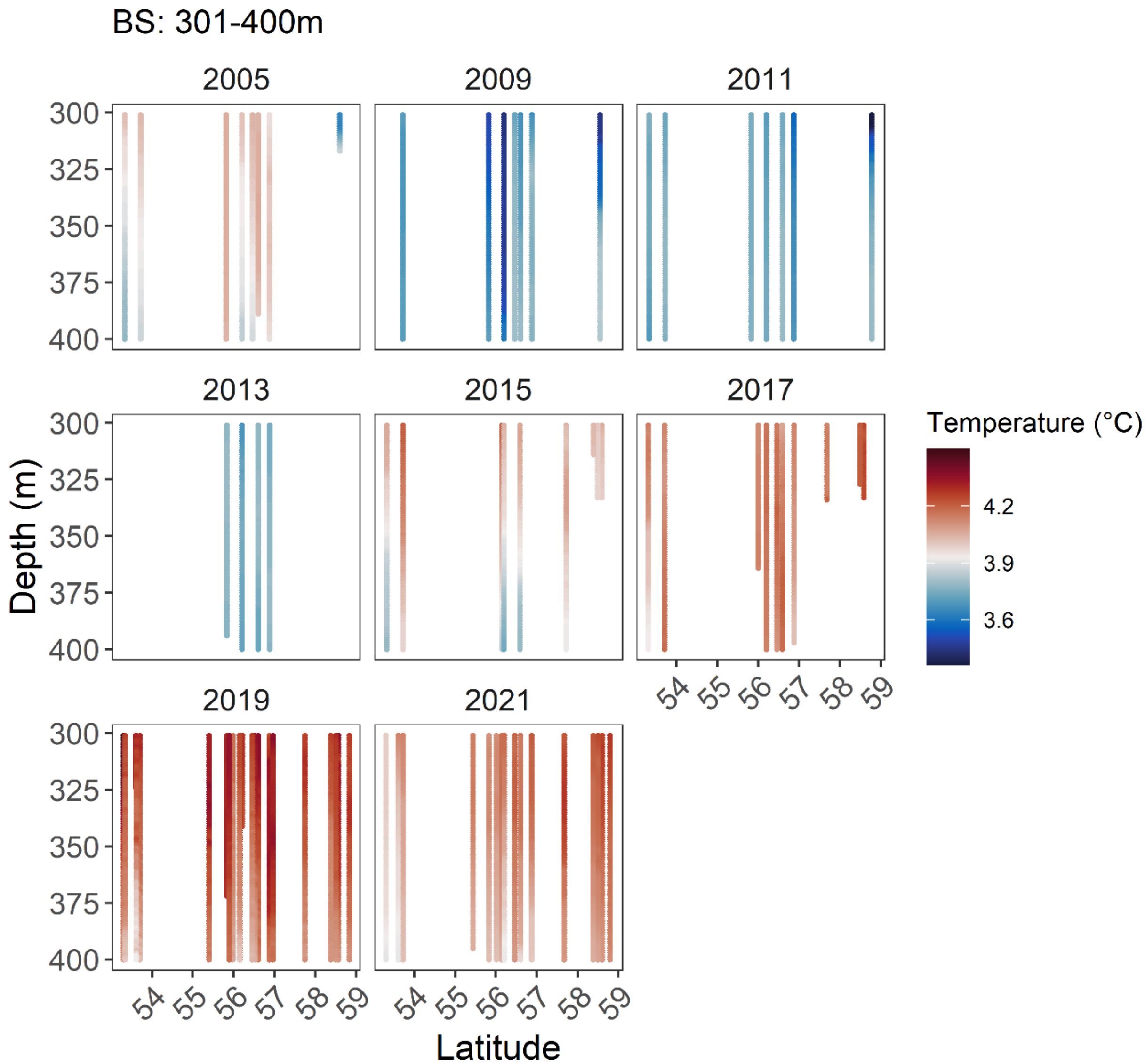

Figure 10. -- Bering Sea temperature (color scale) by year at 1-m increments from depths of 301 to 400 m (y-axis), where the x-axis depicts south to north (left to right).

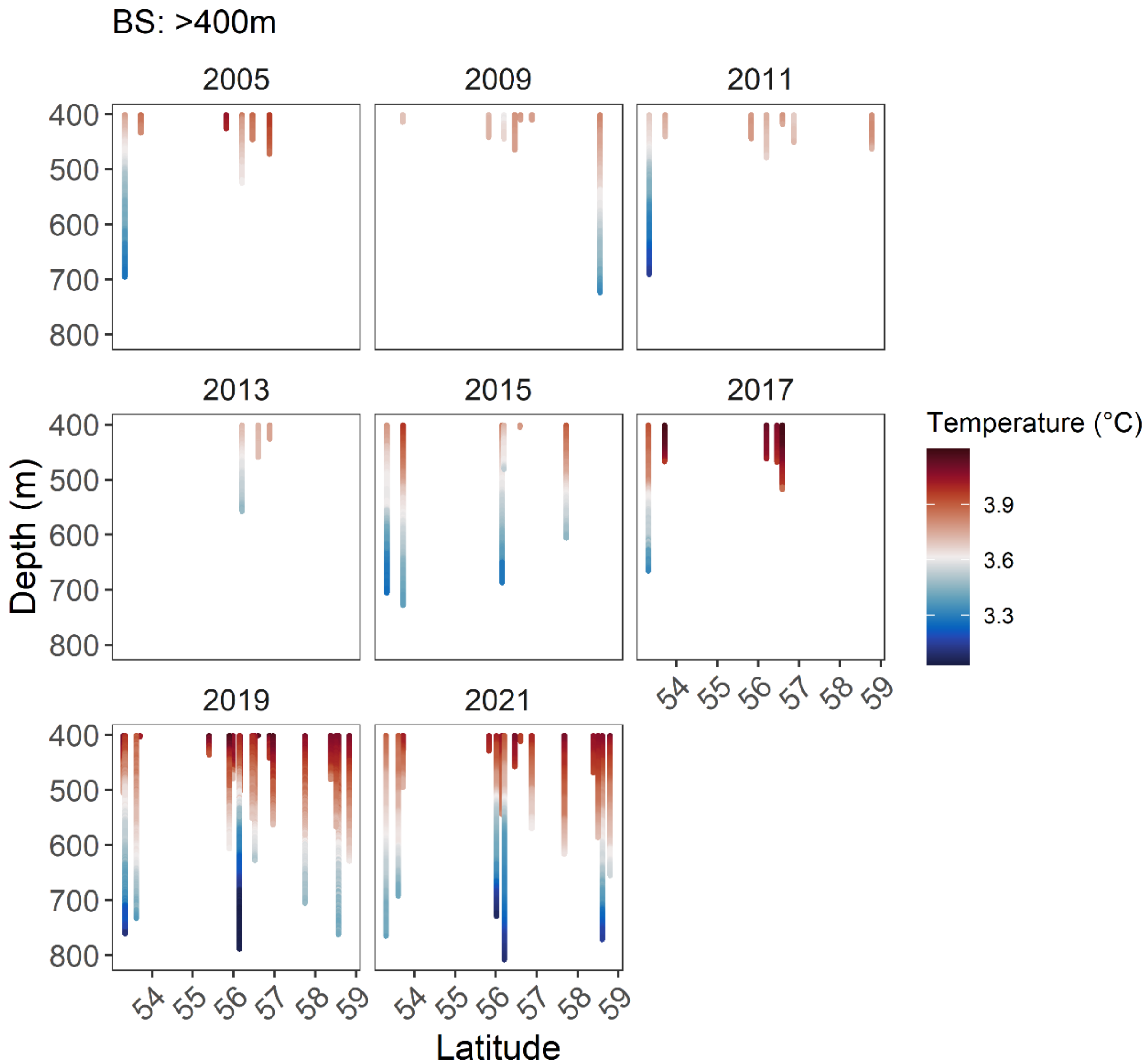

Figure 11. -- Bering Sea temperature (color scale) by year at 1-m increments from depths greater than 400 m (y-axis), where the x-axis depicts south to north (left to right).

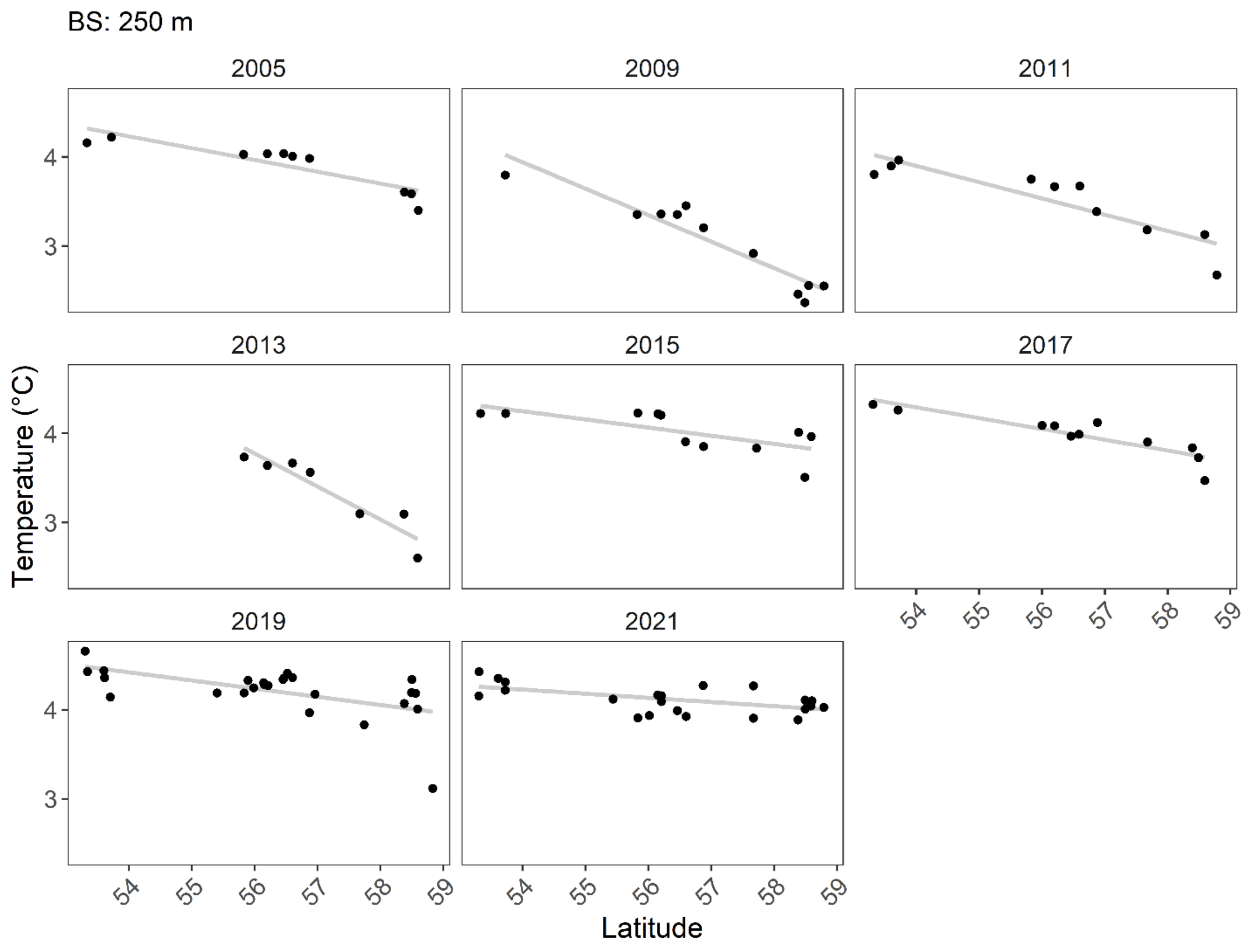

Figure 12. -- Bering Sea temperature at 250 m (mean of the interpolated 1-m increment temperatures from 246 to 255 m), where the x-axis depicts south to north (left to right), and linear trends are shown in light grey.

Gulf of Alaska

Moving from west to east in the GOA (predominantly the northern continental shelf break of the North Pacific Ocean), the general trend is warming from west to east, with interannual variability in subsurface temperatures evident. Interpretation of this trend is difficult, particularly at the surface, because sampling occurs in late June in the WGOA, moving from ~169 to 156.25°W longitude, while sampling in July and August progresses from ~132 to 156.25°W longitude (Fig. 1), and surface waters warm throughout the summer. These temperatures are those experienced by the survey, but transitions at or near 156.25°W longitude are most likely related to this sampling design artifact. Near surface waters (11–50 m) in the WGOA are cooler than those in the CGOA and EGOA, with an overall cool period evident from 2006 through 2013; temperatures in 2021 were cooler relative to other recent years (Fig. 13). At depths from 51 to 200 m this trend remains (Figs. 14 and 15), and at depths from 201 to 300 m there is even cooler water present in 2010, particularly the CGOA and EGOA (Fig. 16). The temperatures are relatively constant across years and by regions deeper than 300 m (Figs. 17 and 18). Inclusion of the second TDR deployment starting in 2019 extends the vertical and horizontal range of temperatures recorded by the AFSC longline survey (Figs. 16–18). For one subsurface depth layer (mean of the interpolated 1-m increment temperatures from 246 to 255 m), there remains a general warming from west to east, though variability and the effect that sampling date has on water temperatures at this depth are not constant (Fig. 19); 2010 is unique in that the WGOA was relatively warm compared to the relatively cooler CGOA (Figs. 16 and 19).

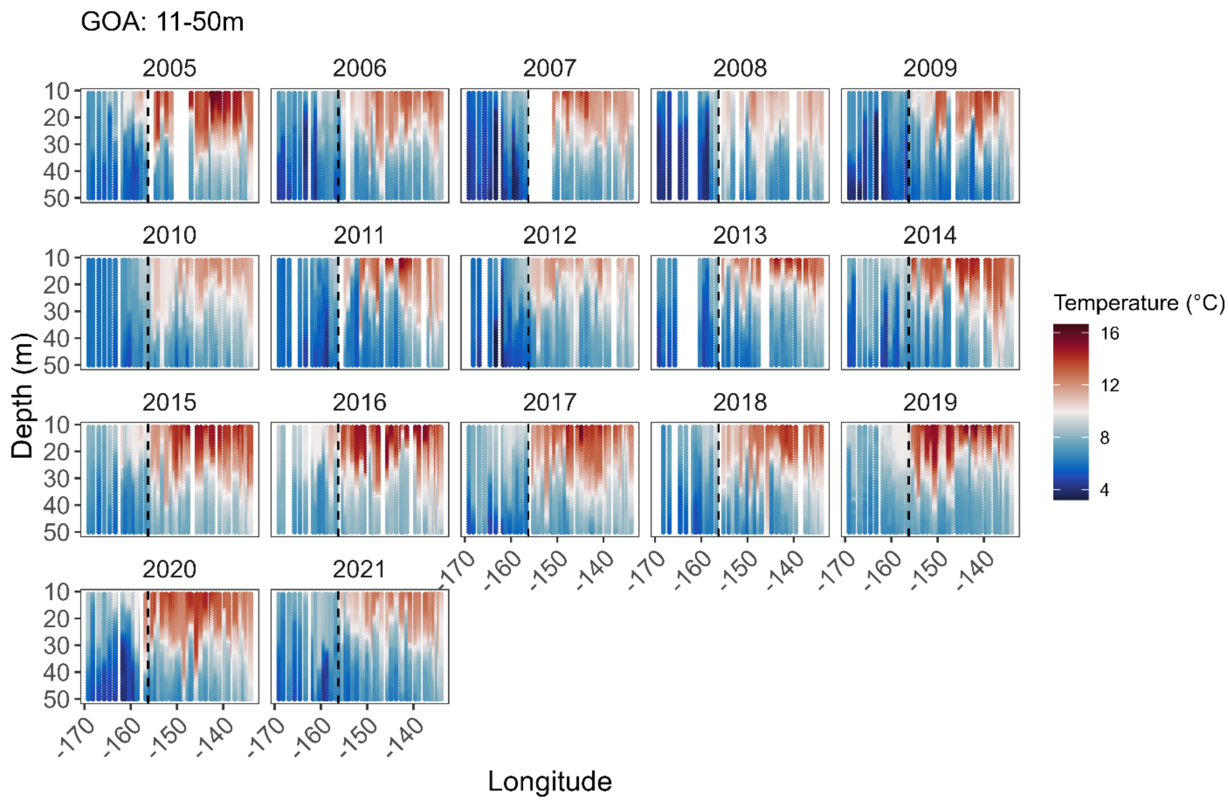

Figure 13. -- Gulf of Alaska temperature (color scale) by year at 1-m increments from depths of 11 to 50 m (y-axis), where the x-axis depicts west to east (left to right). Vertical dashed line at 156.25°W longitude indicates the transition of the survey sampling from west to east left of the line, to east to west right of the line.

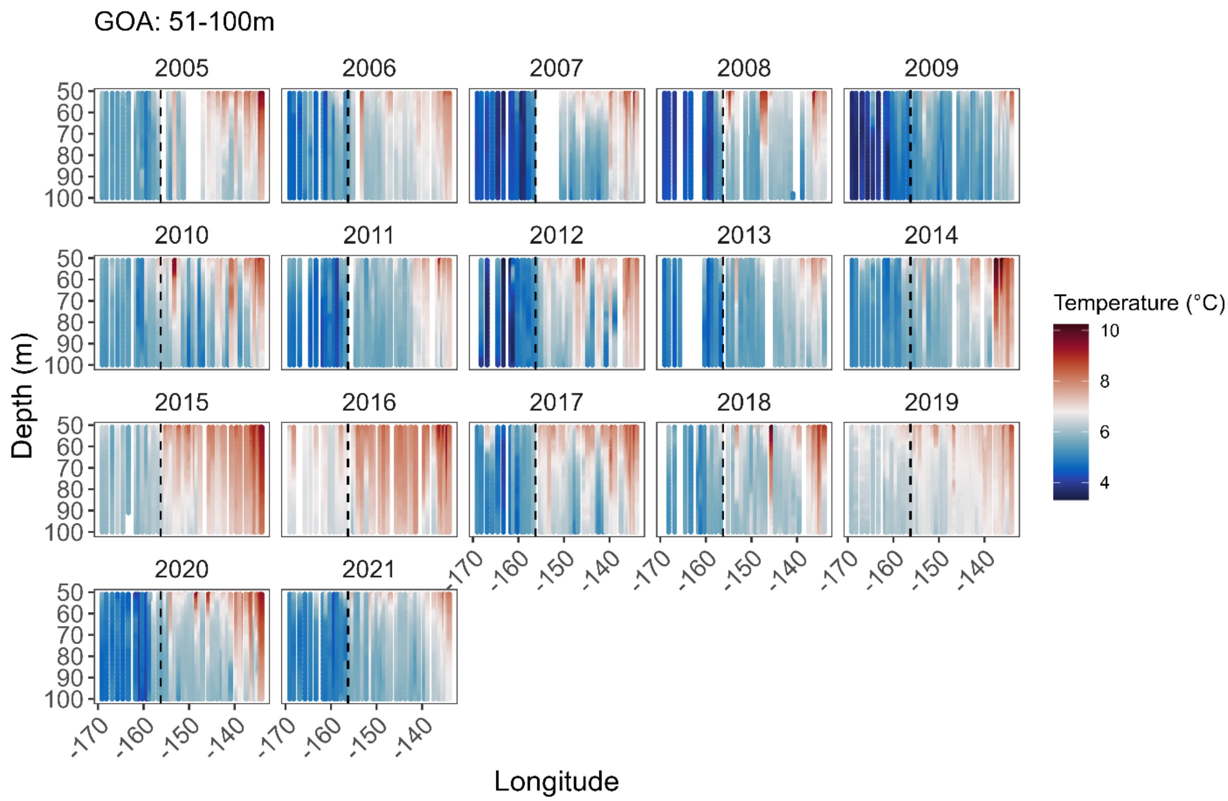

Figure 14. -- Gulf of Alaska temperature (color scale) by year at 1-m increments from depths of 51 to 100 m (y-axis), where the x-axis depicts west to east (left to right). Vertical dashed line at 156.25°W longitude indicates the transition of the survey sampling from west to east left of the line, to east to west right of the line.

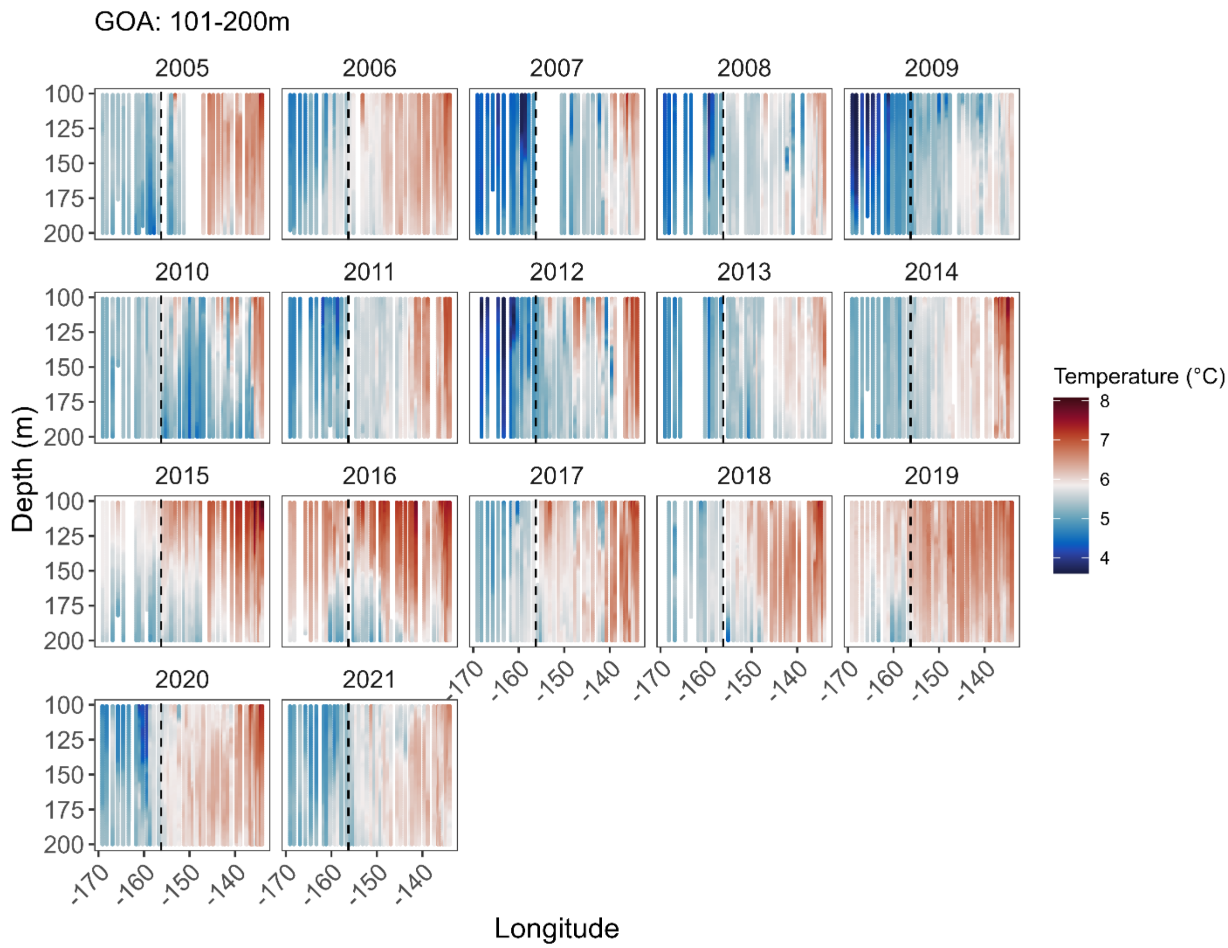

Figure 15. -- Gulf of Alaska temperature (color scale) by year at 1-m increments from depths of 101 to 200 m (y-axis), where the x-axis depicts west to east (left to right). Vertical dashed line at 156.25°W longitude indicates the transition of the survey sampling from west to east left of the line, to east to west right of the line.

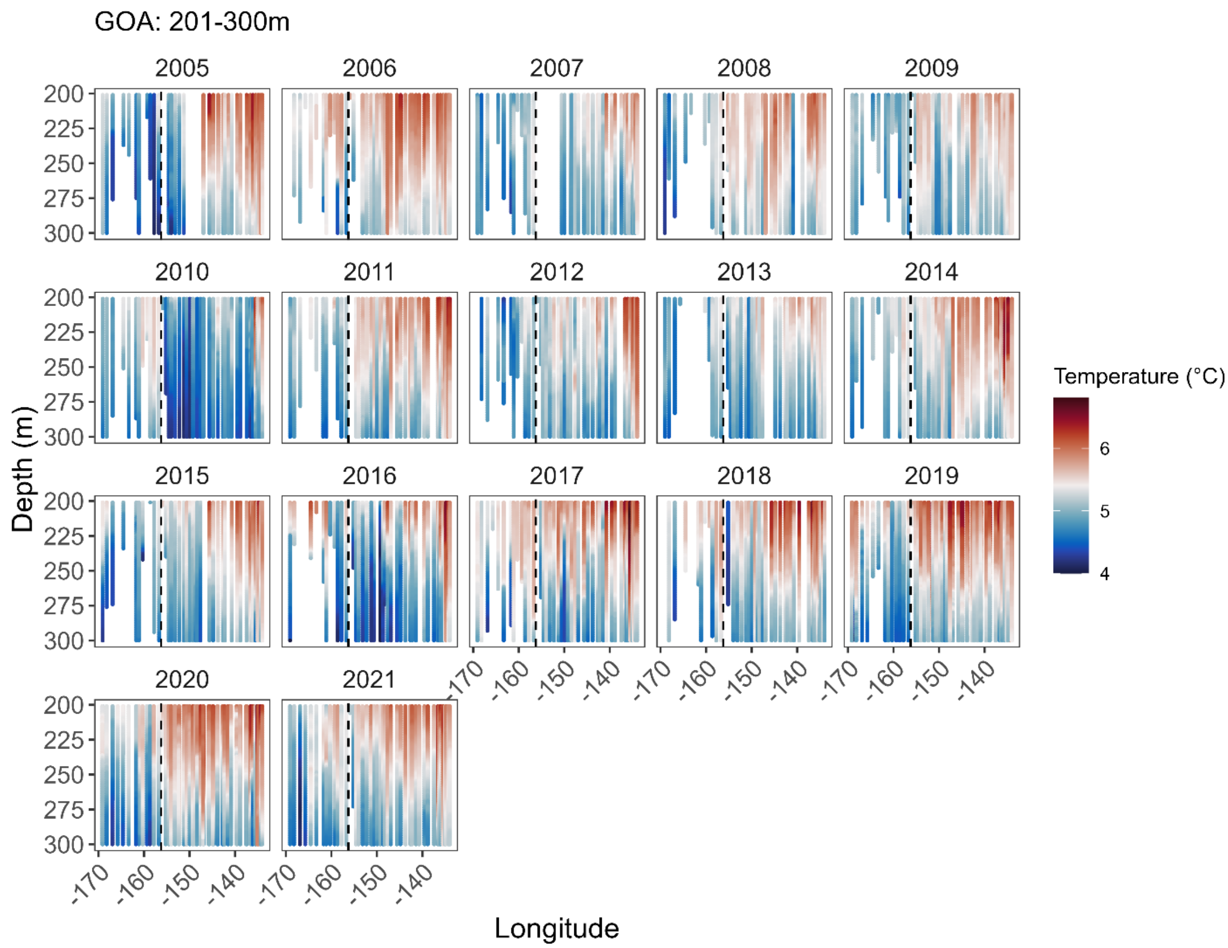

Figure 16. -- Gulf of Alaska temperature (color scale) by year at 1-m increments from depths of 201 to 300 m (y-axis), where the x-axis depicts west to east (left to right). Vertical dashed line at 156.25°W longitude indicates the transition of the survey sampling from west to east left of the line, to east to west right of the line.

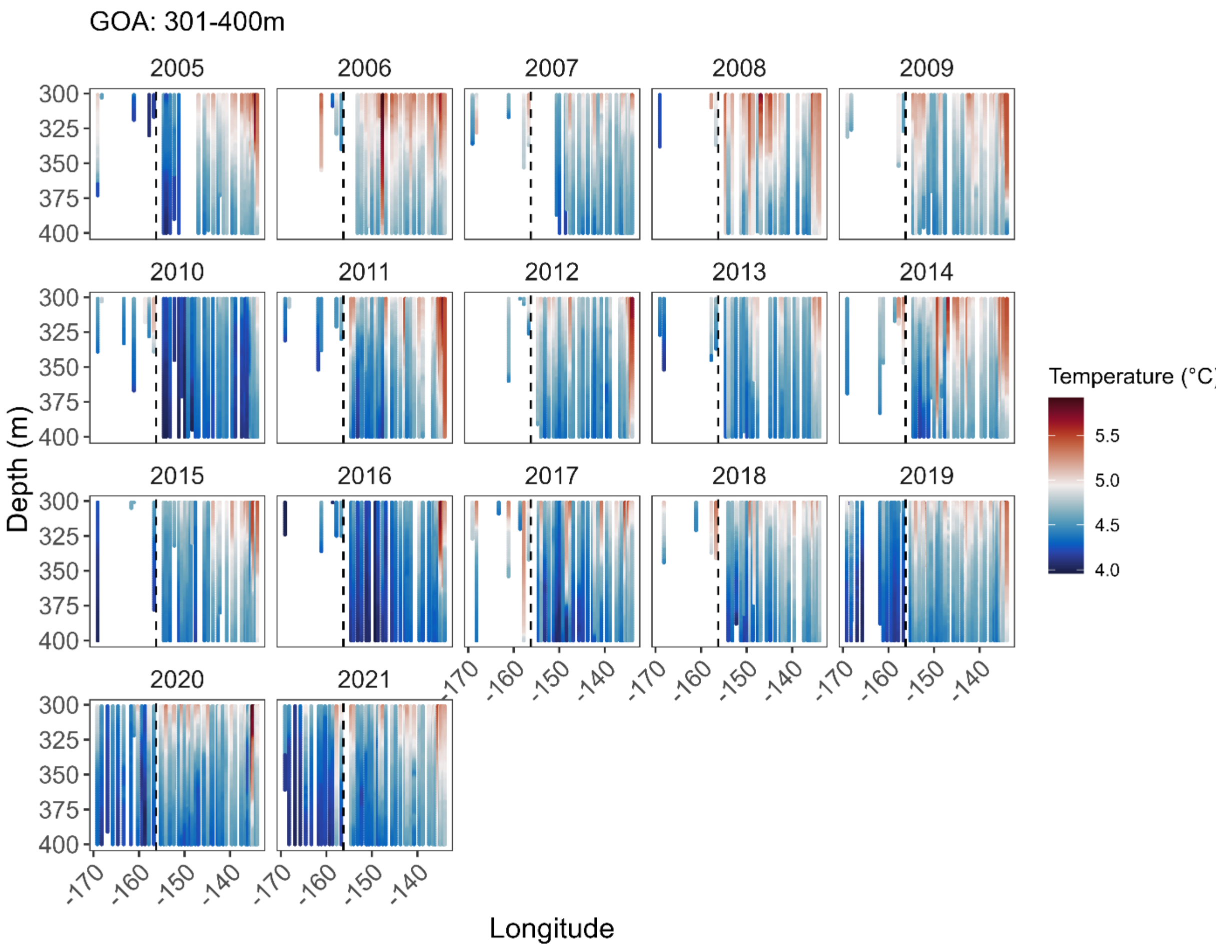

Figure 17. -- Gulf of Alaska temperature (color scale) by year at 1-m increments from depths of 301 to 400 m (y-axis), where the x-axis depicts west to east (left to right). Vertical dashed line at 156.25°W longitude indicates the transition of the survey sampling from west to east left of the line, to east to west right of the line.

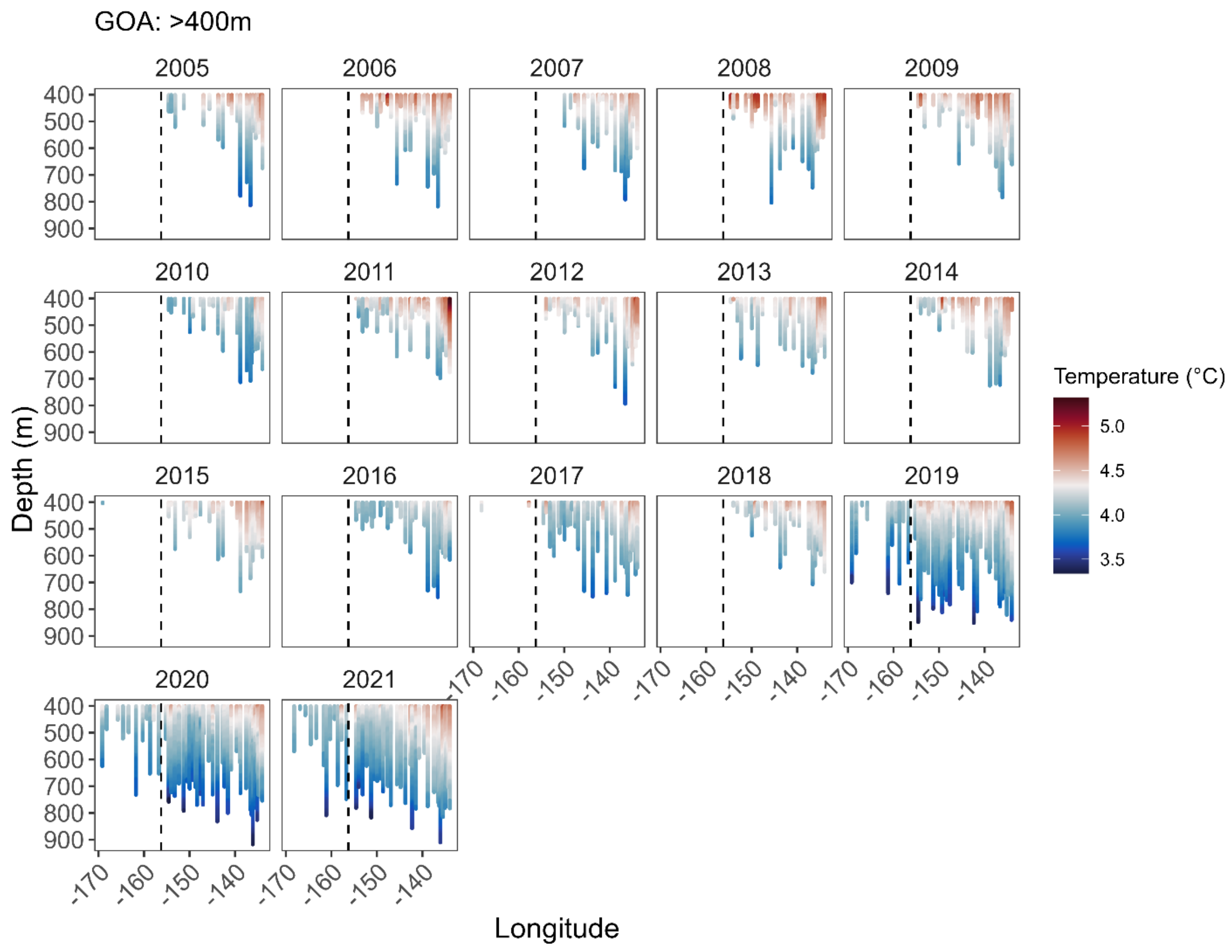

Figure 18. -- Gulf of Alaska temperature (color scale) by year at 1-m increments from depths greater than 400 m (y-axis), where the x-axis depicts west to east (left to right). Vertical dashed line at 156.25°W longitude indicates the transition of the survey sampling from west to east left of the line, to east to west right of the line.

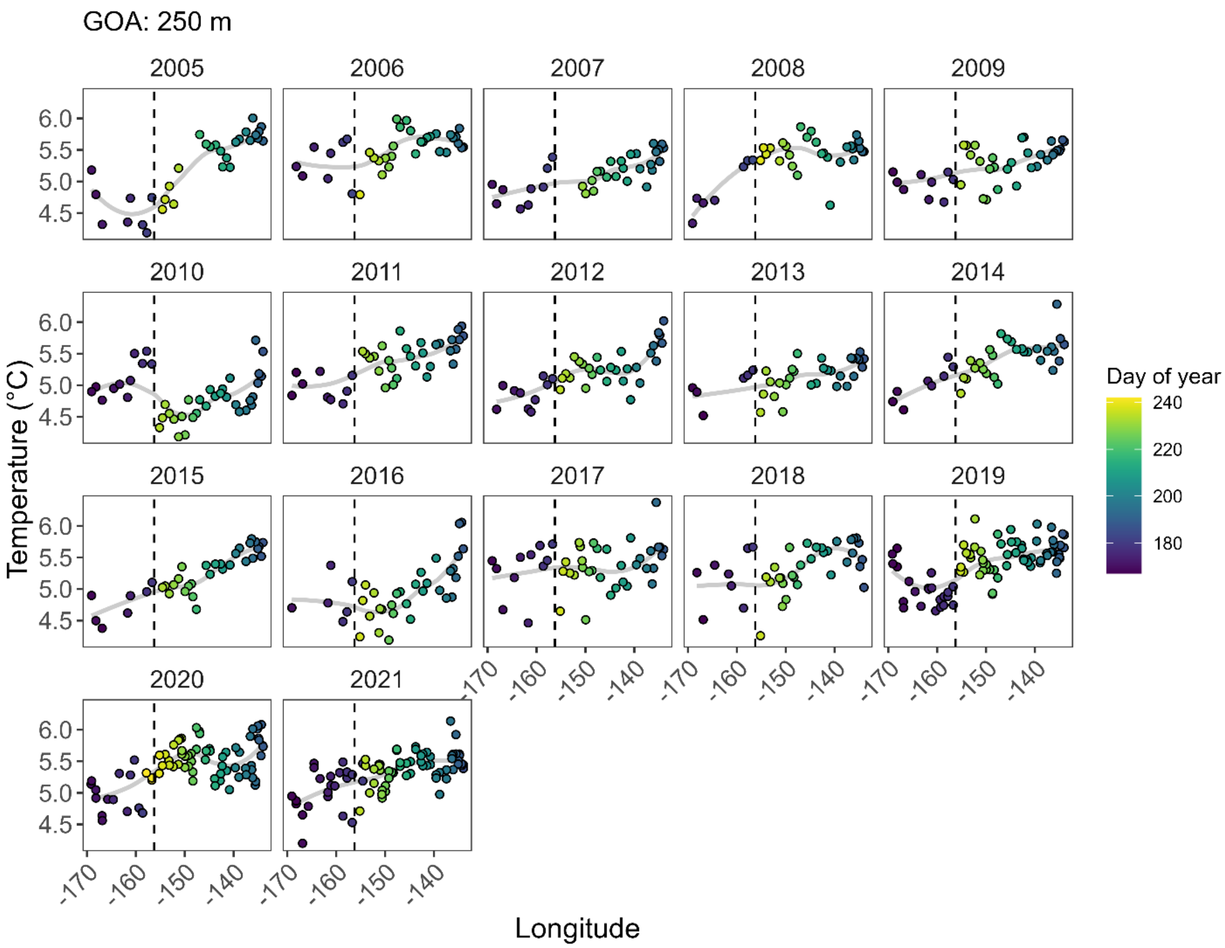

Figure 19. -- Gulf of Alaska temperature at 250 m (y-axis is the mean of the interpolated 1-m increment temperatures from 246 to 255 m), where the x-axis depicts west to east (left to right), the sampling date is reflected by the color (day of year), and localized smooth trends are shown in light grey. Vertical dashed line at 156.25°W longitude indicates the typical transition of the survey sampling from west to east left of the line, to east to west right of the line.

Aleutian Islands

In the AI, differences in subsurface temperatures exist between north and south of the island chain, and there is much more variability longitudinally, which may be related to the numerous passes connecting the GOA and BS. While the longline survey sampled the AI in 2010, subsurface temperature was not available from this leg of the survey and is thus absent from this summary. In the shallower 11 to 50-m layer, subsurface water was slightly cooler north of the chain, and there is a clear split showing 2006, 2008, and 2012 are relatively cool and 2014, 2016, 2018, and 2020 are relatively warm (Fig. 20). As the depth increases, the range of temperature decreases, but the same pattern remains (Figs. 21–25). Inclusion of the second TDR deployment starting in 2020 for this region extends the vertical and horizontal range of temperatures recorded by the AFSC longline survey (Fig. 25). When focusing on one subsurface depth layer (mean of the interpolated 1-m increment temperatures from 246 to 255 m), temperature south of the chain appears more constant or even slightly increasing from west to east, while subsurface temperature north of the chain may have a decreasing trend from west to east (Fig. 26). There is evidence that 2020 was a warmer year in the AI time series and not in the GOA highlighting differences across the North Pacific Ocean.

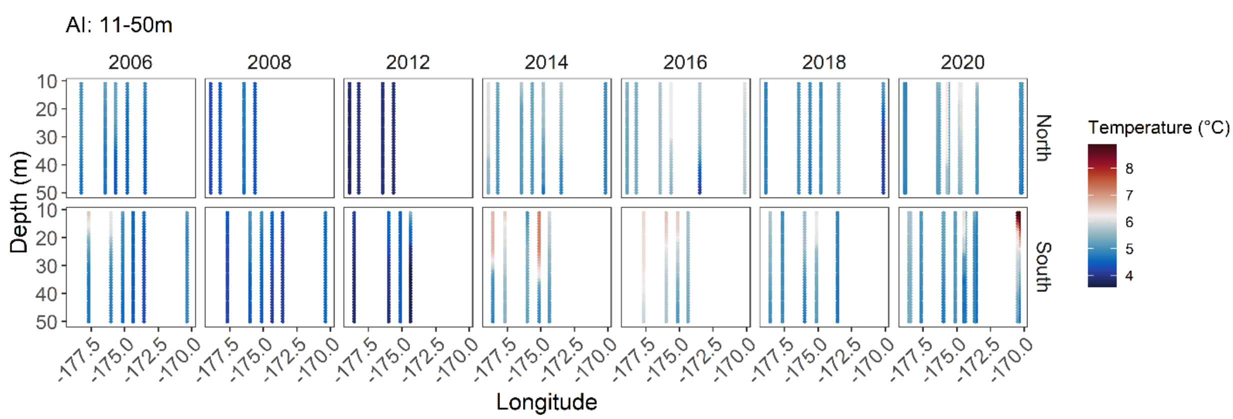

Figure 20. -- Aleutian Islands temperature (color scale) by year at 1-m increments from depths of 11 to 50 meters (y-axis), where the x-axis depicts west to east (left to right). The top panel shows stations from north of the island chain, and the bottom panel shows stations from south of the island chain.

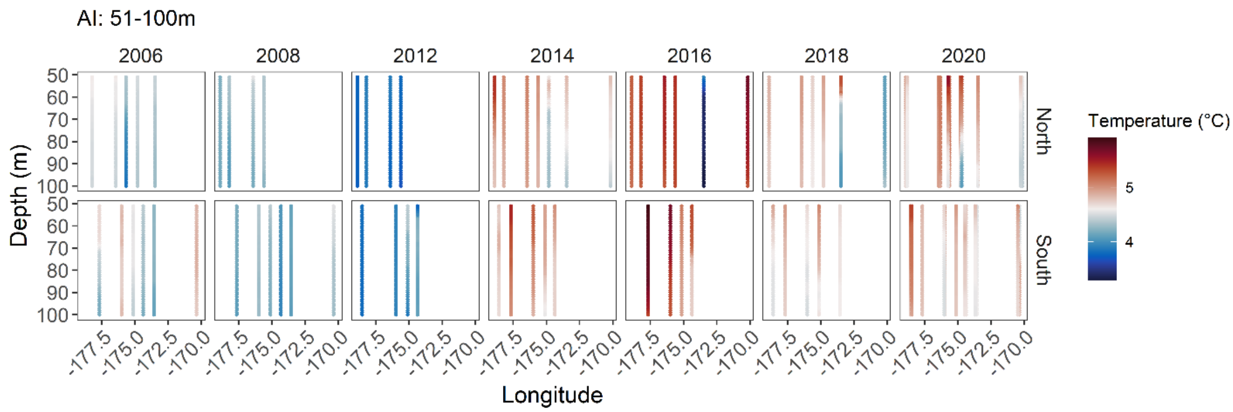

Figure 21. -- Aleutian Islands temperature (color scale) by year at 1-m increments from depths of 51 to 100 m (y-axis), where the x-axis depicts west to east (left to right). The top panel shows stations from north of the island chain, and the bottom panel shows stations from south of the island chain.

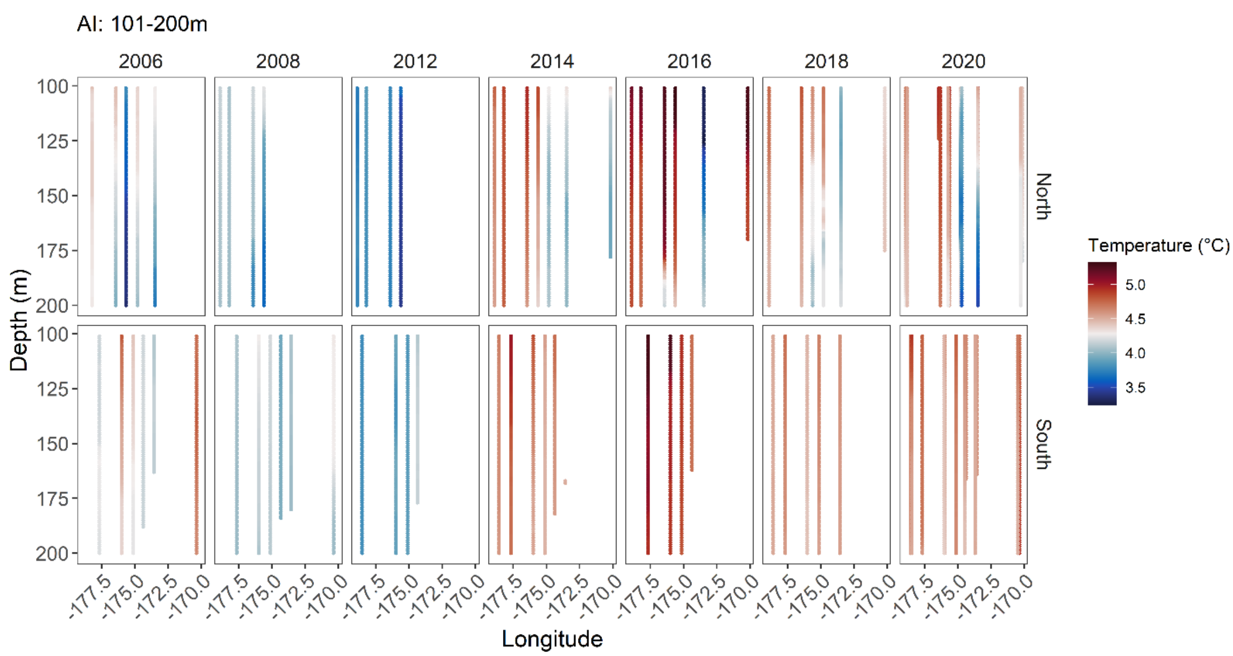

Figure 22. -- Aleutian Islands temperature (color scale) by year at 1-m increments from depths of 101 to 200 m (y-axis), where the x-axis depicts west to east (left to right). The top panel shows stations from north of the island chain, and the bottom panel shows stations from south of the island chain.

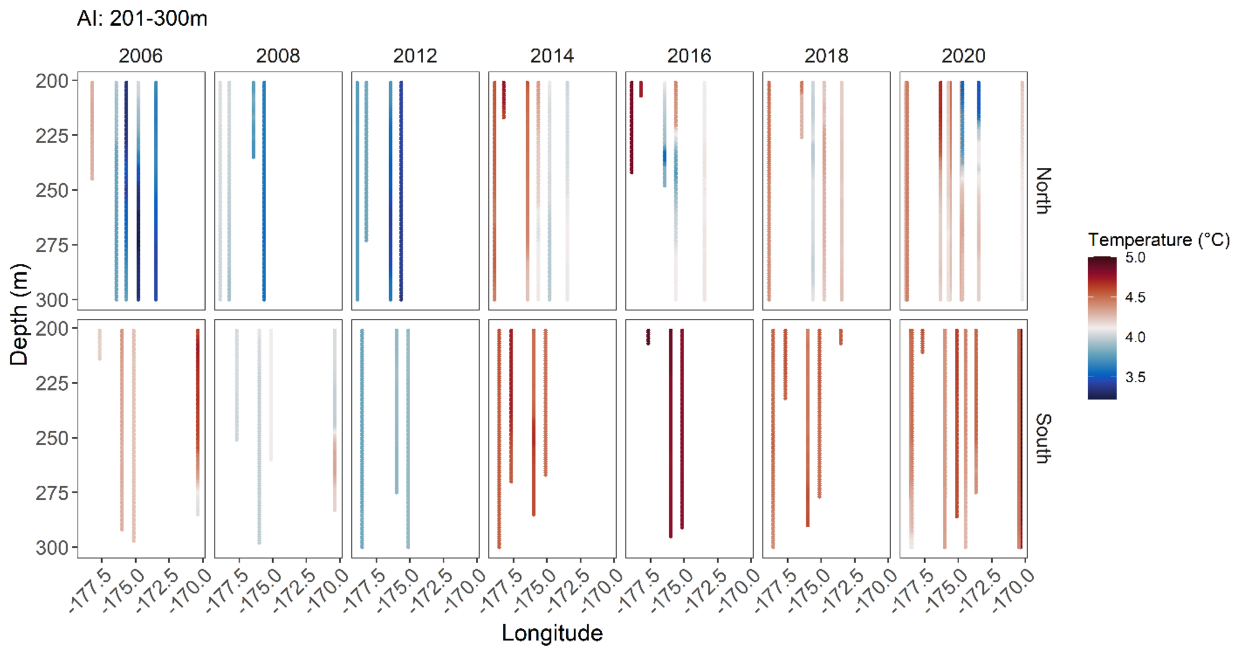

Figure 23. -- Aleutian Islands temperature (color scale) by year at 1-m increments from depths of 201 to 300 m (y-axis), where the x-axis depicts west to east (left to right). The top panel shows stations from north of the island chain, and the bottom panel shows stations from south of the island chain.

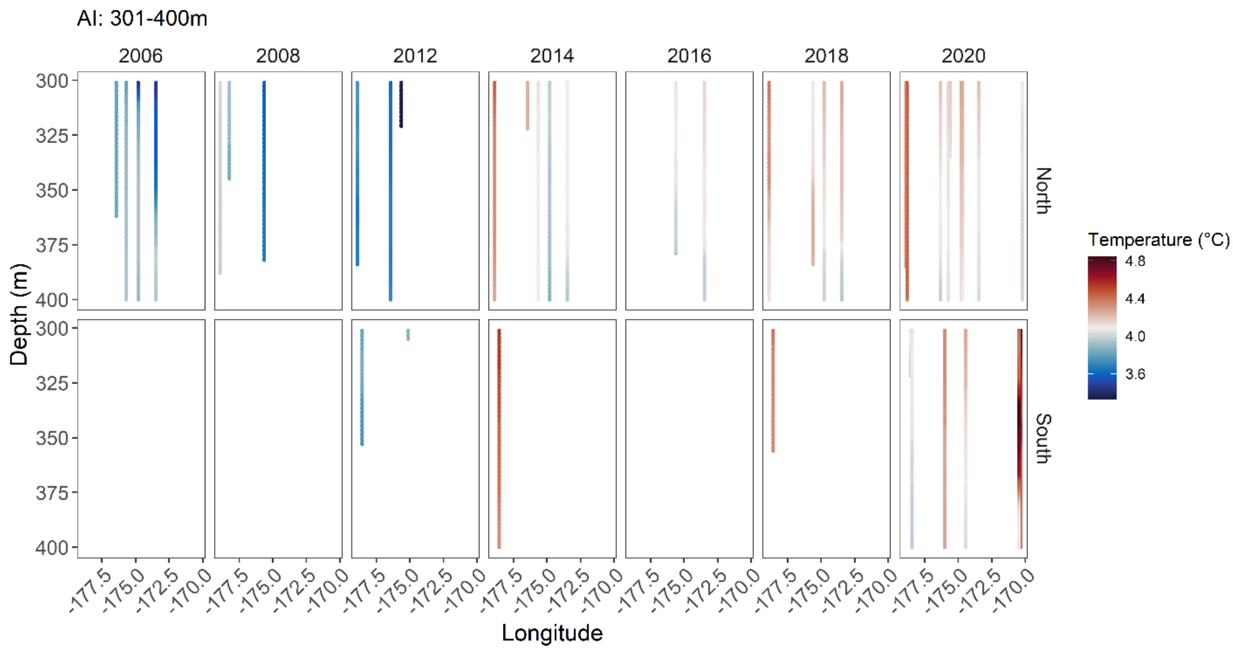

Figure 24. -- Aleutian Islands temperature (color scale) by year at 1-m increments from depths of 301 to 400 m (y-axis), where the x-axis depicts west to east (left to right). The top panel shows stations from north of the island chain, and the bottom panel shows stations from south of the island chain.

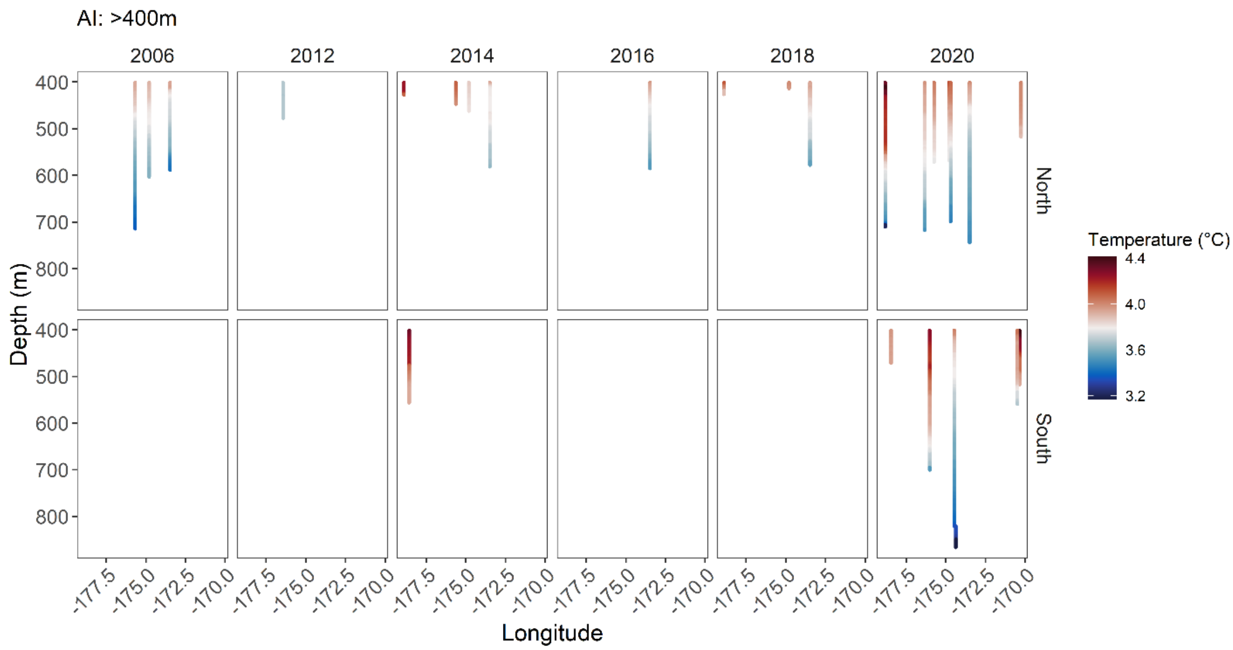

Figure 25. -- Aleutian Islands temperature (color scale) by year at 1-m increments from depths greater than 400 m (y-axis), where the x-axis depicts west to east (left to right). The top panel shows stations from north of the island chain, and the bottom panel shows stations from south of the island chain. Note that there was no data deeper than 400 m in 2008.

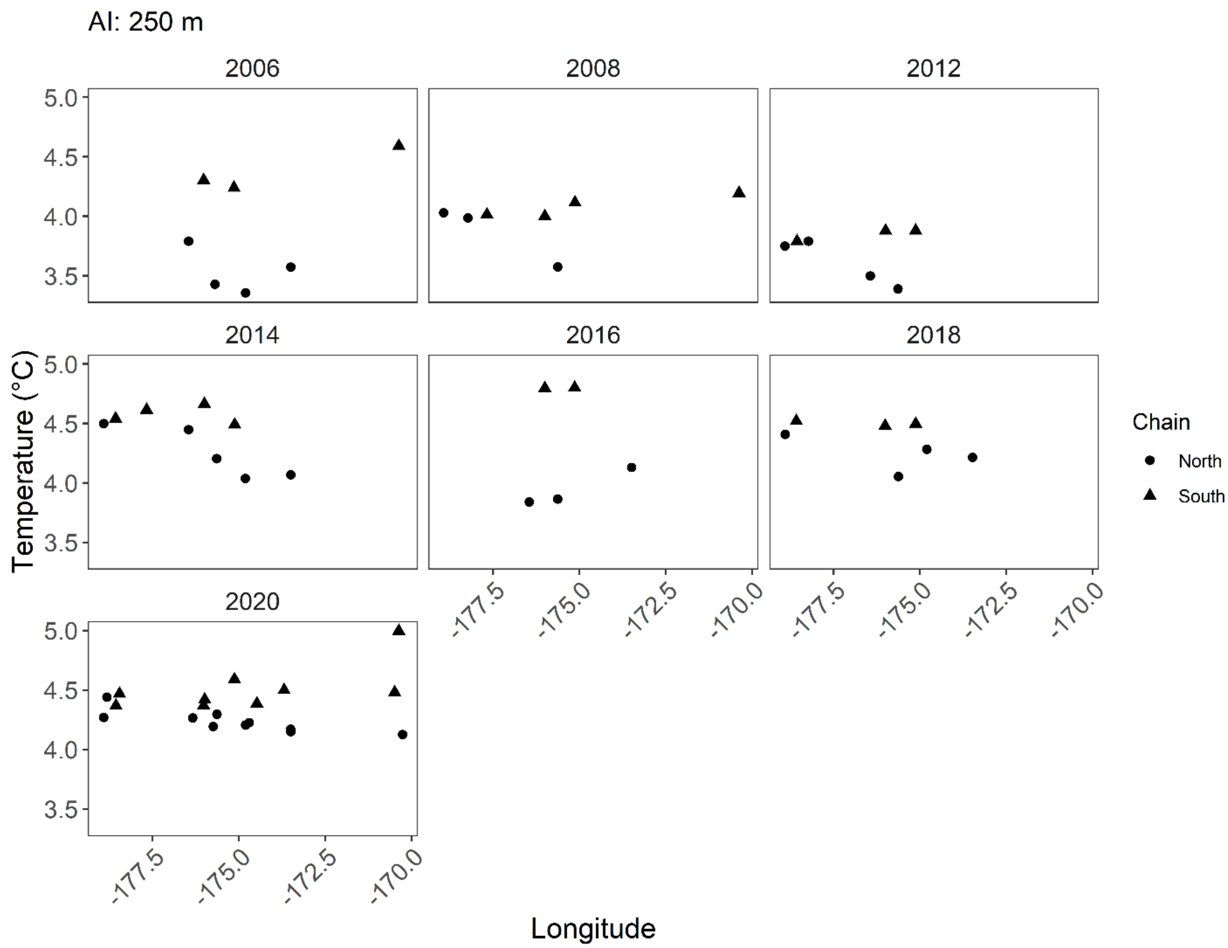

Figure 26. -- Aleutian Islands temperature at 250 m (mean of the interpolated 1-m increment temperatures from 246 to 255 m), where the x-axis depicts west to east (left to right). Circles represent stations from north of the island chain, while triangles represent stations from south of the island chain.

Bottom Temperature Summary

Because the AFSC longline survey occurs along the continental shelf break, a region with sharp bathymetric relief, annual measurements of bottom temperature will not be consistently measured across space and time. The exact latitude and longitude of the TDR deployment at any given station will vary each year due to currents and winds experienced during the setting of longline gear. Bottom water temperature is strongly correlated with bottom depth; therefore, bottom depth is an important consideration for assessing interannual variability in bottom temperature. Bottom temperatures will be summarized by region, and comparisons will be made with temperature-depth profiles.

Between 2005 and 2021, there were 1,356 hauls with complete haul information and processed TDR bottom temperature data, which includes 174 deeper second set TDR deployments starting in 2019. Bathymetry is inherently associated with station location. As a result, the probability that a specific depth is sampled by a TDR varies across the five regions, and the bottom temperatures observed relate to geography and bathymetry in addition to inter-annual variability. For example, the warmest regional median bottom temperature occurs in the WGOA where the mean TDR depth is shallowest, but the coolest regional mean bottom temperature occurs in the BS where sea ice contributes to cooler water temperatures (Fig. 27). When focusing on just the deeper second set data, similar patterns are present over a narrower range of temperature and depth (Fig. 28).

Bottom temperature is the mean of two or more hours of sampling, and the range from the minimum and maximum temperature recorded during that period provide a metric for how much variability is occurring. These ranges in bottom temperature are generally in line with the variability of midwater temperatures observed in profiles of the same region (Figs. 29–33). The highest variability in bottom temperatures was in the WGOA when depth was less than 400 m, and there may be more variability with depth in the EGOA (Fig. 34). The probability of very high bottom temperature ranges seems to have a slight increase during relatively warm years (2015, 2016, and 2019), and the probability distribution of bottom temperature range appears to shift slightly greater in the deeper second set compared to the shallower first set (Fig. 35), though the reason for this difference in not known.

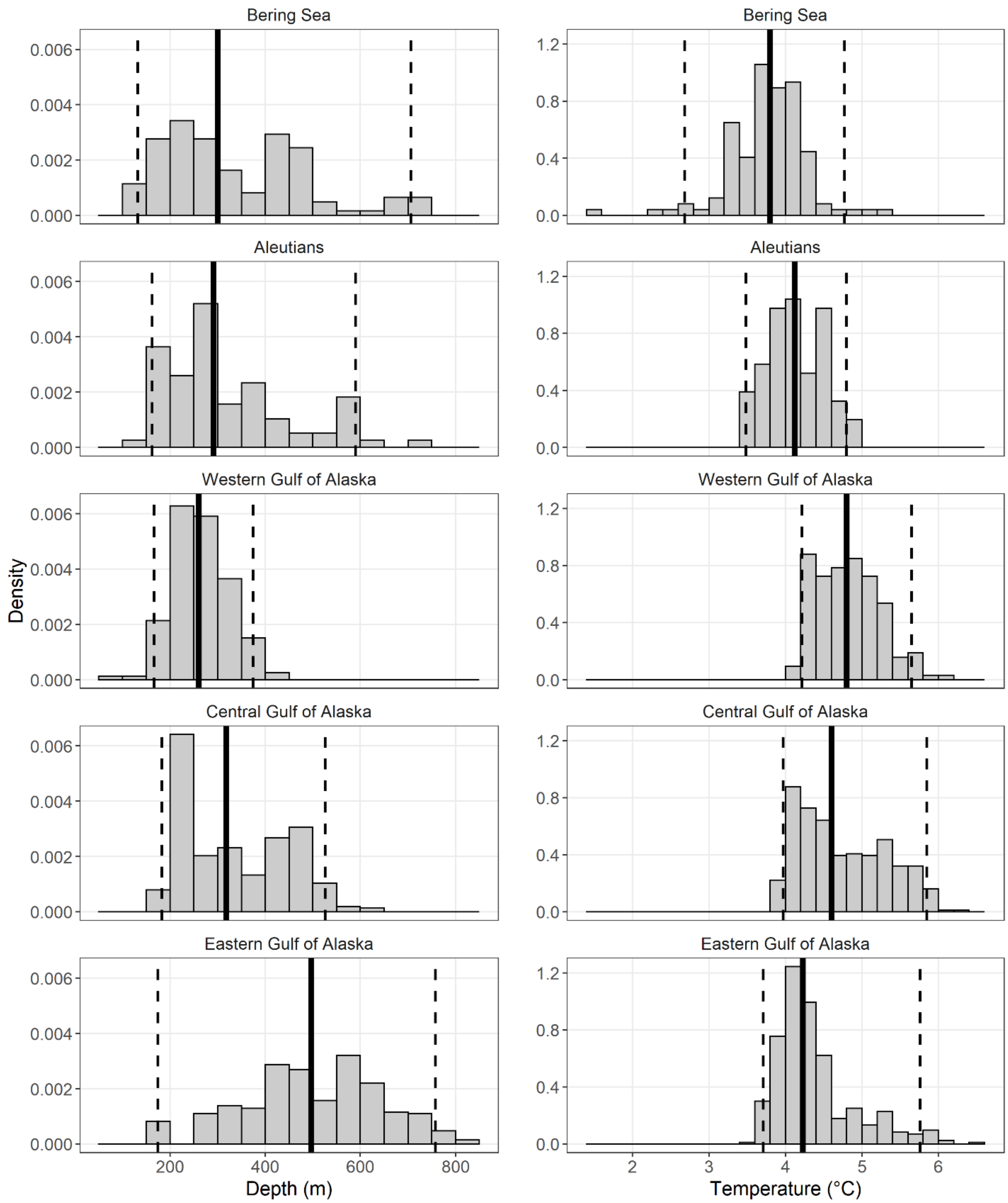

Figure 27. -- The probability distribution by geographic regions of bottom depth (left) and bottom temperature (right) recorded daily from the temperature and depth recorder on the first haul on the Alaska Fisheries Science Center longline survey from 2005 to 2021. The solid vertical lines indicates the median value, while the dashed vertical lines coincide with the 2.5% and 97.5% quantiles. Bin widths are 50 m for depth and 0.2 °C for temperature.

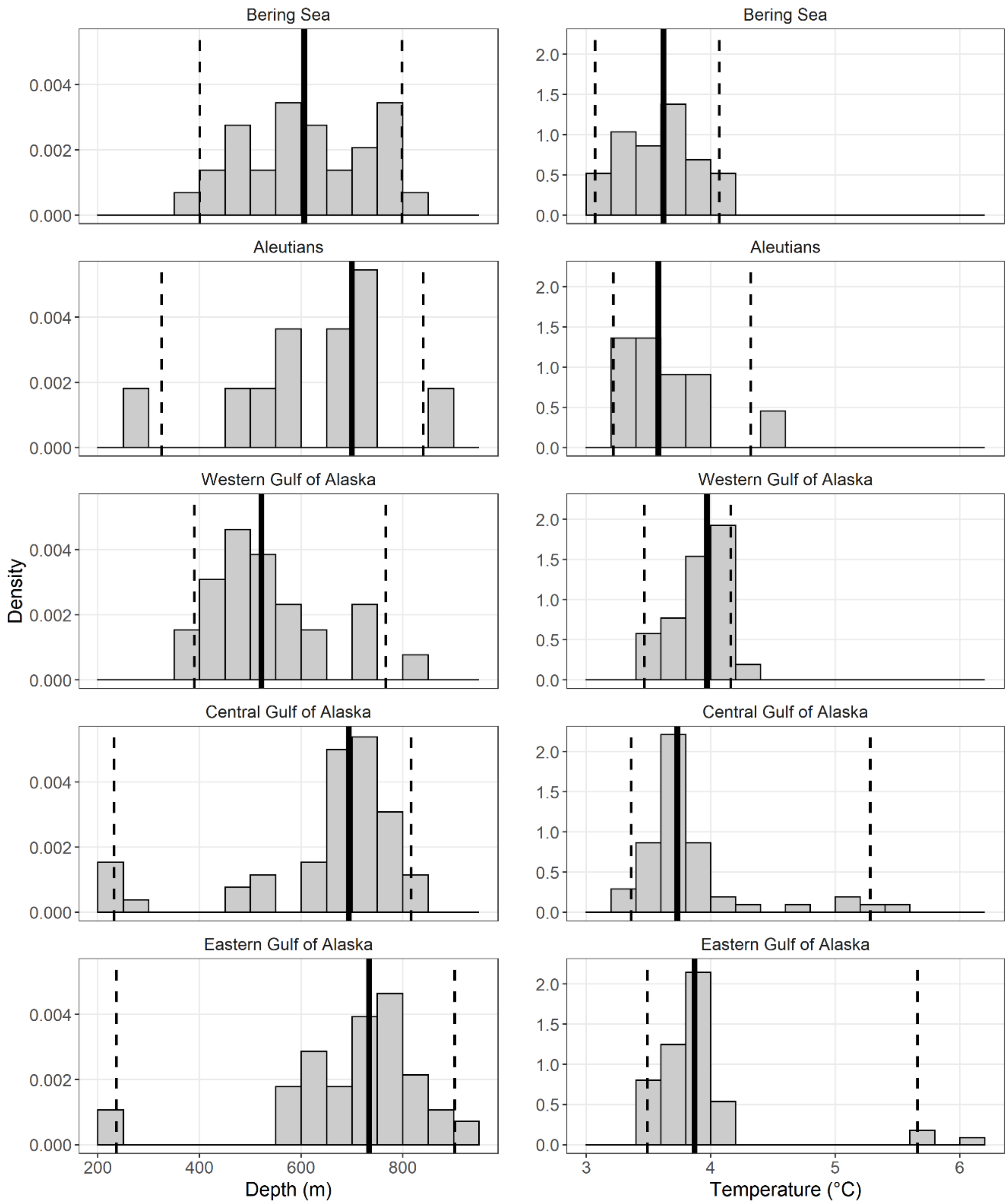

Figure 28. -- The probability distribution by geographic regions of bottom depth (left) and bottom temperature (right) recorded daily from the temperature and depth recorder on the second haul (generally deeper) on the Alaska Fisheries Science Center longline survey from 2019 to 2021. The solid vertical lines indicates the median value, while the dashed vertical lines coincide with the 2.5% and 97.5% quantiles. Bin widths are 50 m for depth and 0.2 °C for temperature.

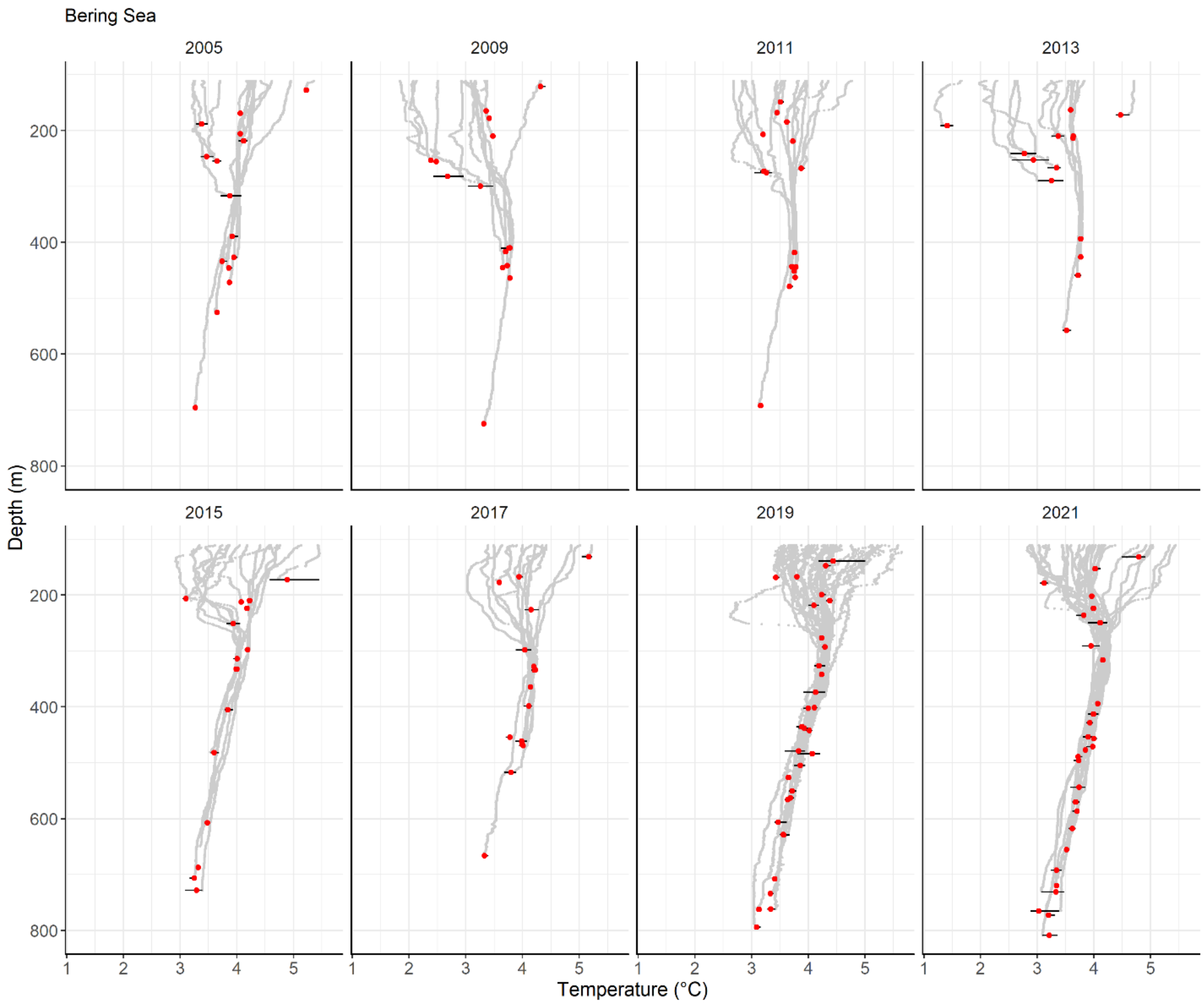

Figure 29. -- The annual co-occurrence of midwater temperature-depth profiles (gray points), mean bottom temperature (red points), and range of temperatures while on the bottom (horizontal black lines) in the Bering Sea. Note the increase in deep samples beginning in 2019 with the addition of a TDR on the second set.

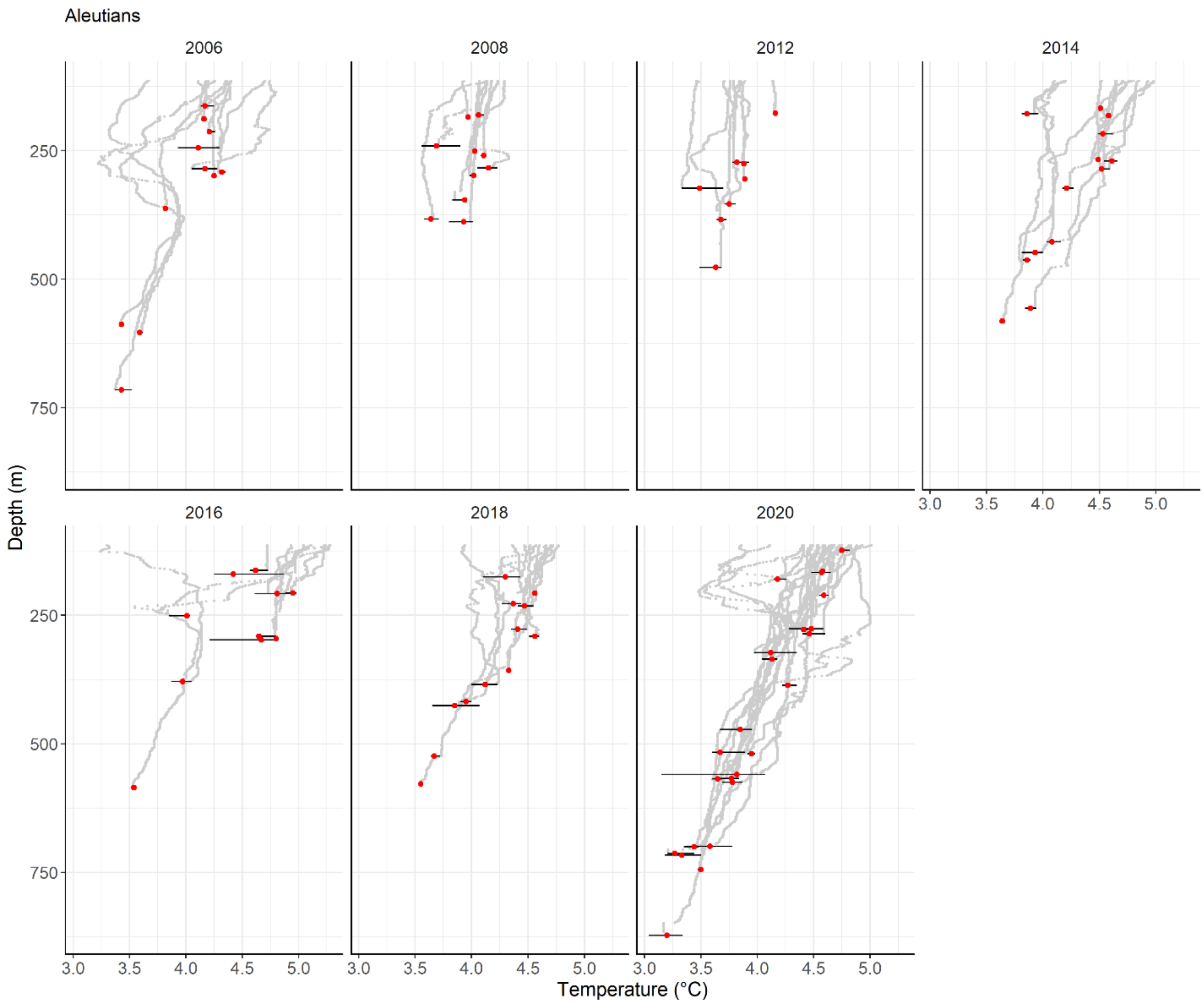

Figure 30. -- The annual co-occurrence of temperature-depth profiles (gray points), mean bottom temperature (red points), and range of temperatures while on the bottom (horizontal black lines) in the Aleutian Islands. Note the increase in deep samples beginning in 2019 with the addition of a TDR on the second set.

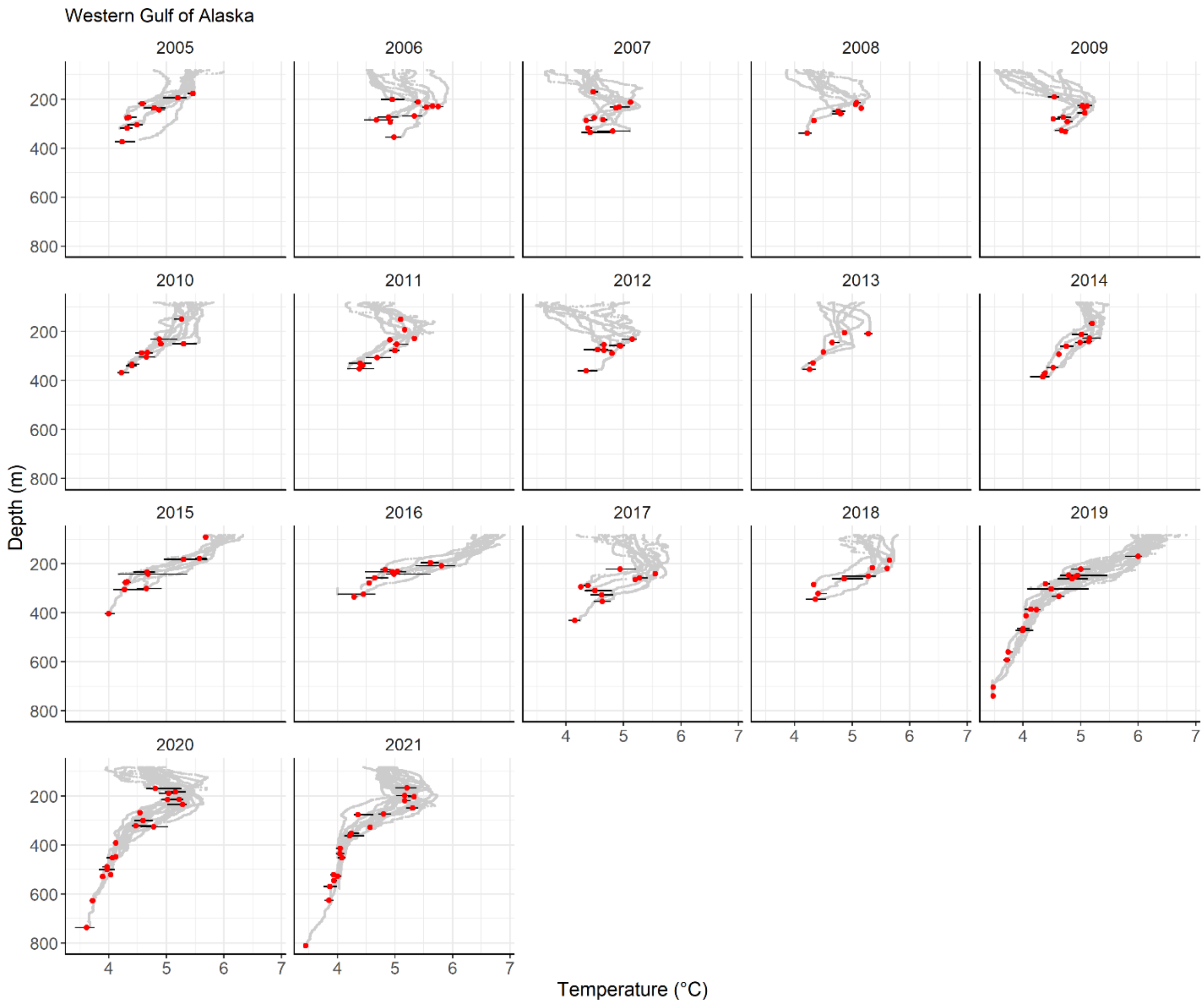

Figure 31. -- The annual co-occurrence of temperature-depth profiles (gray points), mean bottom temperature (red points), and range of temperatures while on the bottom (horizontal black lines) in the western Gulf of Alaska. Note the increase in deep samples beginning in 2019 with the addition of a TDR on the second set.

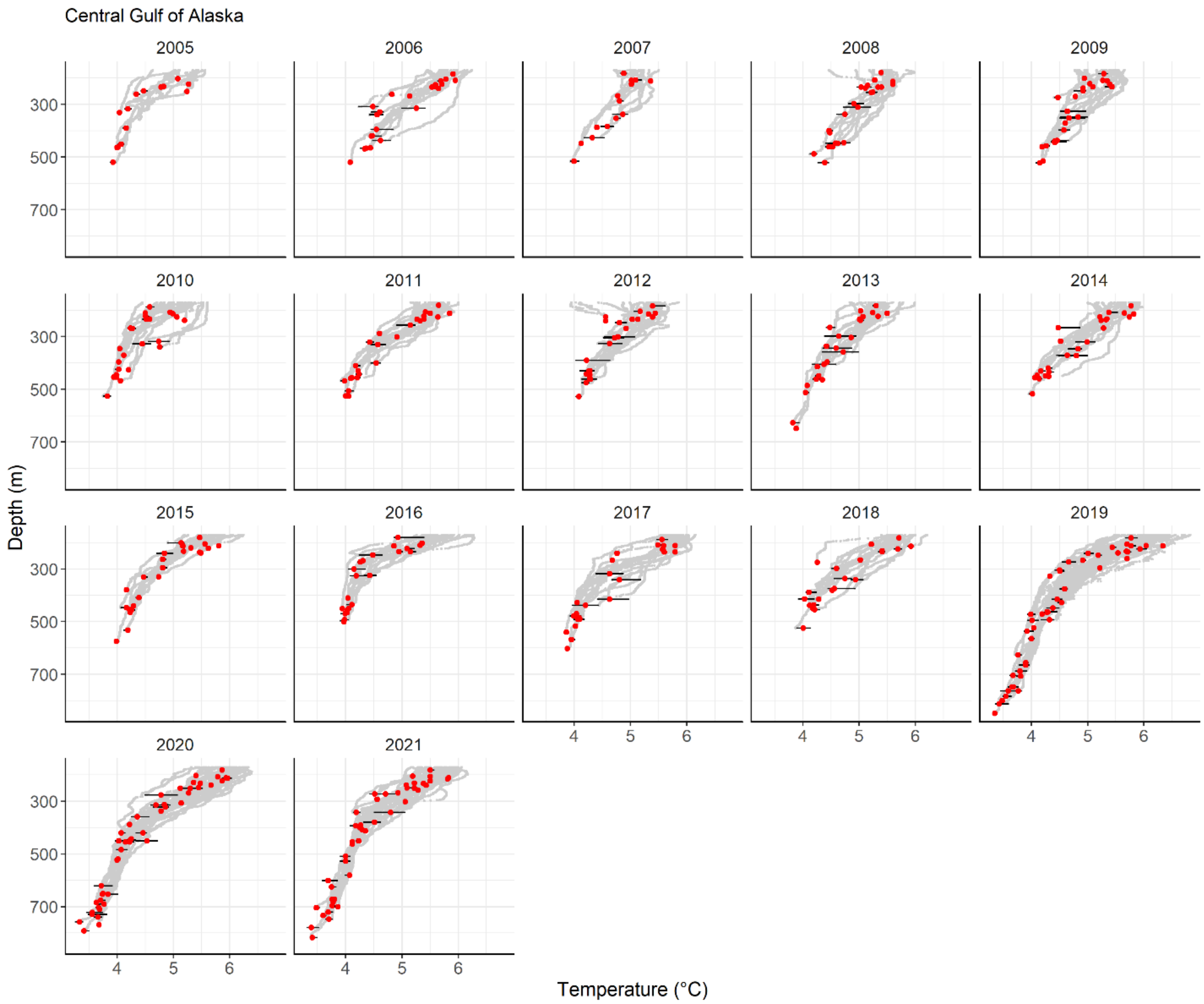

Figure 32. -- The annual co-occurrence of temperature-depth profiles (gray points), mean bottom temperature (red points), and range of temperatures while on the bottom (horizontal black lines) in the central Gulf of Alaska. Note the increase in deep samples beginning in 2019 with the addition of a TDR on the second set.

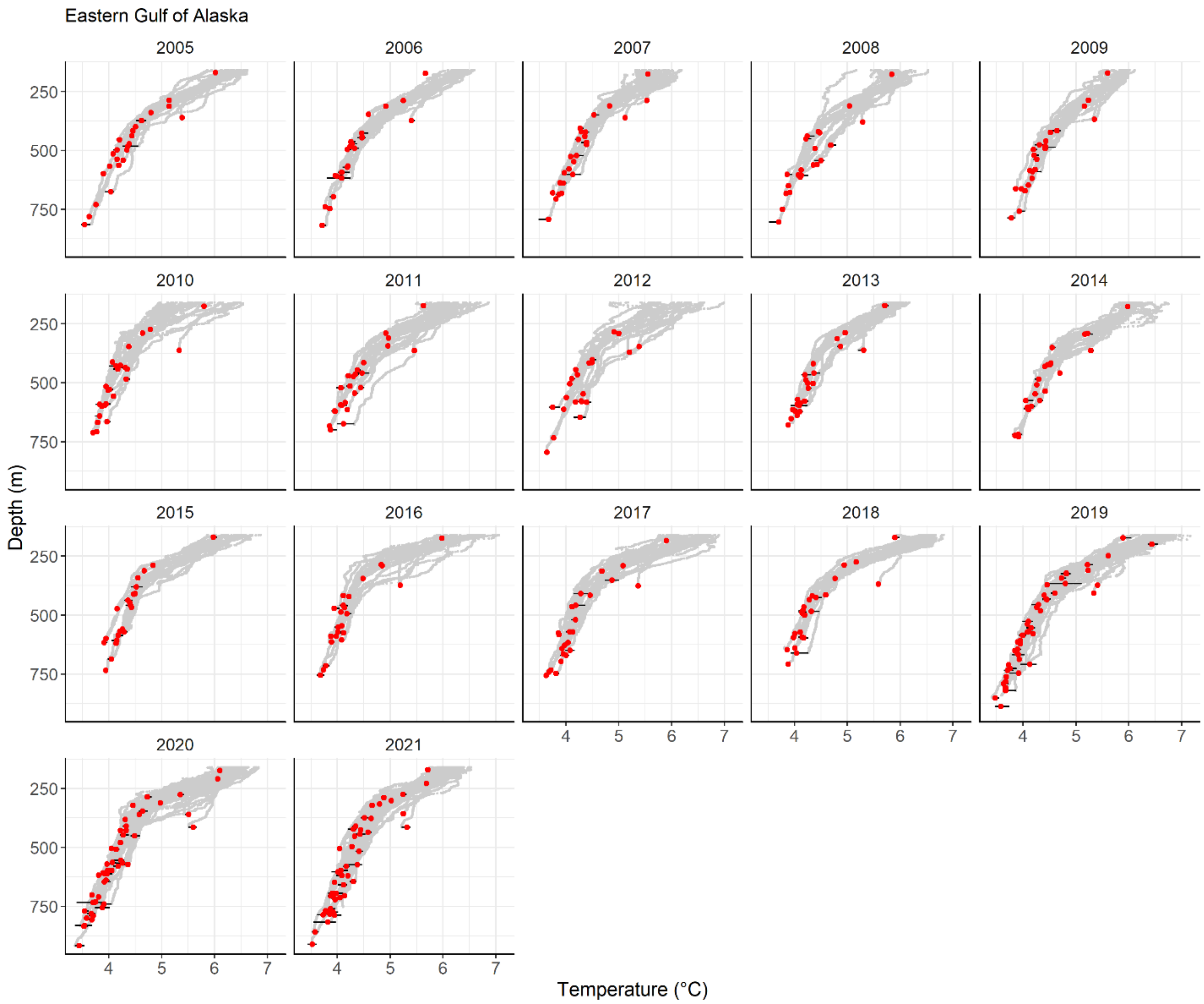

Figure 33. -- The annual co-occurrence of temperature-depth profiles (gray points), mean bottom temperature (red points), and range of temperatures while on the bottom (horizontal black lines) in the eastern Gulf of Alaska. Note the increase in deep samples beginning in 2019 with the addition of a TDR on the second set.

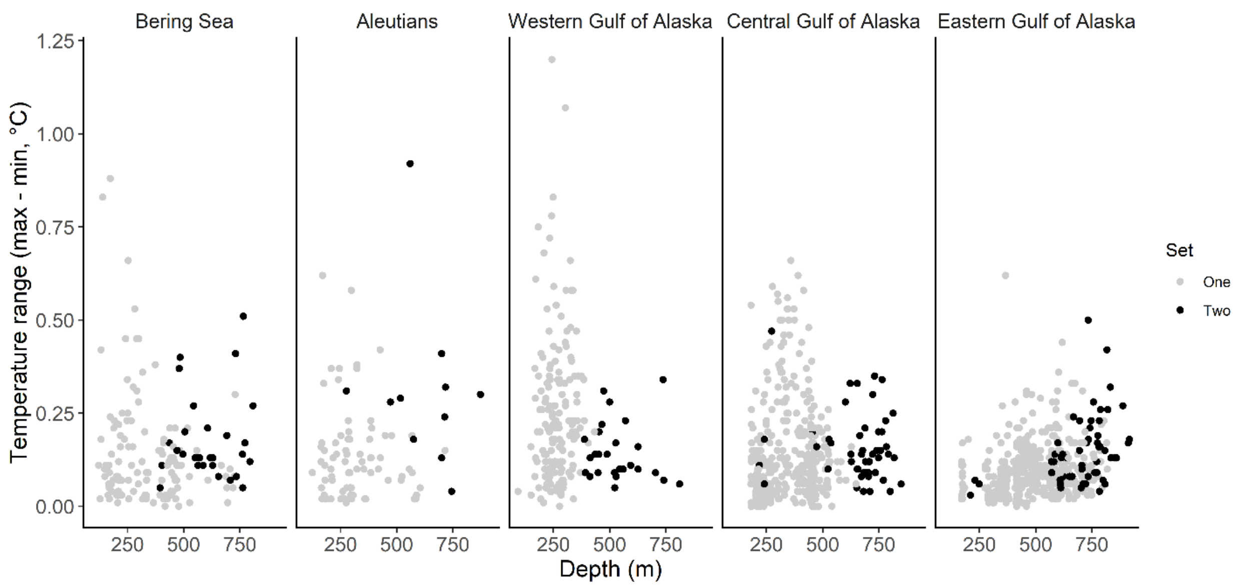

Figure 34. -- Plots of each bottom temperature range (maximum minus minimum) against the mean bottom depth by region, with grey points from the shallower first set and the black points from the deeper second set (beginning in 2019).

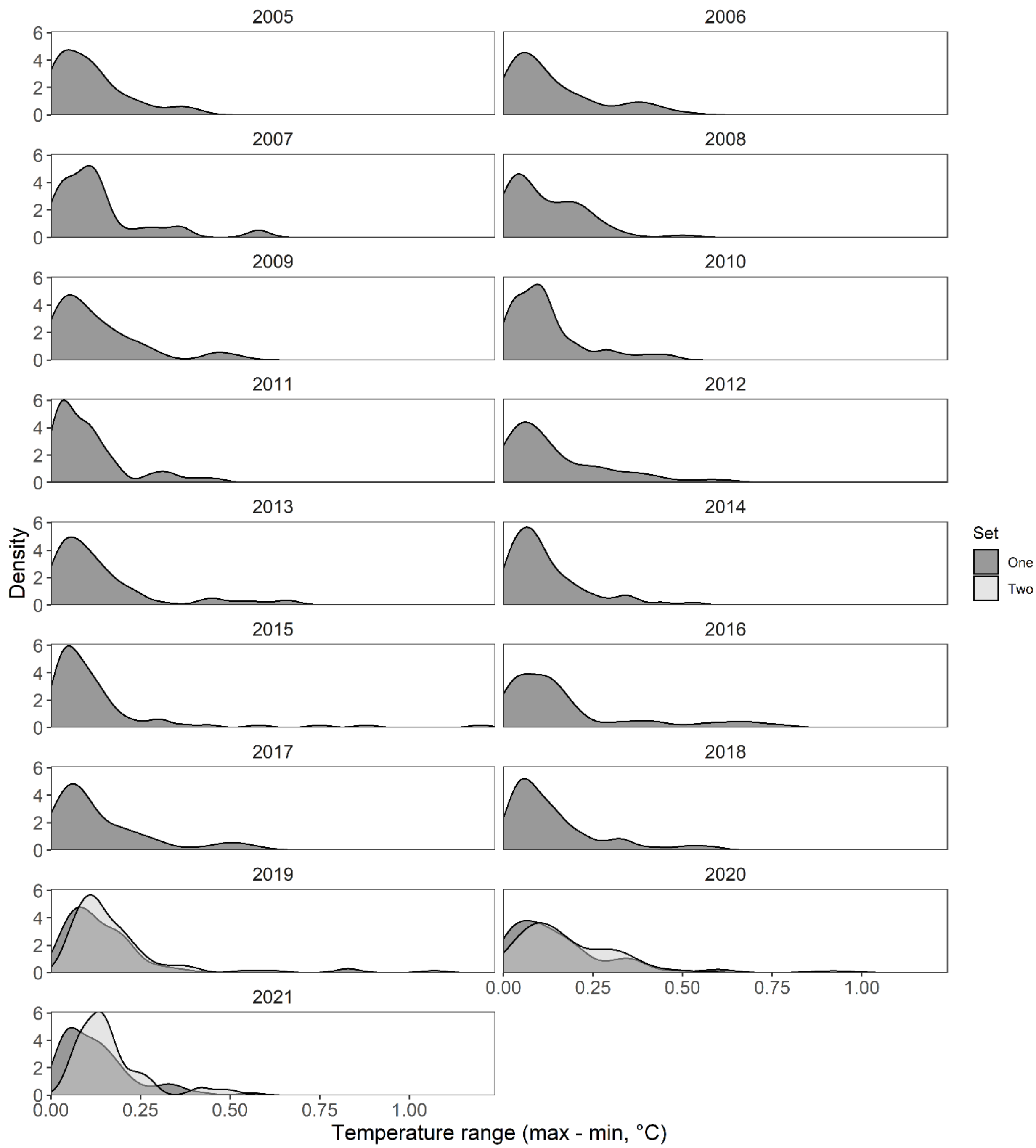

Figure 35. -- Density plots showing bottom temperature range (maximum minus minimum) by year for all areas combined, with dark grey shading from the shallower first set and light grey shading from the deeper second set (beginning in 2019).

SUBSURFACE TEMPERATURE ECOSYSTEM INDICATOR

Subsurface temperature can be a useful indicator for tracking long-term ecosystem trends (i.e., static, cooling, or warming) for groundfish. Unlike sea surface temperature which represents a single discrete layer on the top of the water column, depth must also be considered for subsurface (or bottom) temperature. The AFSC longline survey provides a snapshot of temperature-depth profiles from the continental shelf break across Alaska waters (Figs. 6–25), and this information can be synthesized with other subsurface temperatures to provide in situ ecosystem observations through space and time. A consistent metric for interannual comparisons of subsurface temperatures from the AFSC longline survey was also desired. The mean temperature from 1-m increment depths over the 246–255 m depth range was selected as an index for subsurface temperature because this layer was shallow enough to be consistently sampled across space and time and also deep enough to be below most thermoclines and mixed layer dynamics. If the TDR on haul one for a station was not successful, the TDR on the second haul was used in its place (only available since 2019). Though not synoptic, this subsurface thermal layer was examined at three levels to provide a complete picture of this dataset. First, all stations by year and region are included to show the spread of raw values. Second, a mean of stations sampled every year was calculated, which includes 5 BS stations in odd years (2, 8, 10, 12, and 18), 3 AI stations in even years (39, 57, and 58), 0 WGOA stations, 2 CGOA stations (73 and 74), and 11 EGOA stations (91, 92, 93, 94, 100, 102, 104, 105, 106, 108, and 142) (Fig. 1). Finally, an area-weighted mean was calculated using all stations within smaller geographic areas that comprise each management region described in Echave et al. (2013) treated as replicates and weighted by area size (the area used was for depth stratum of 200–300 m) and calculated as:

$$T_{ky} = \frac{\sum_j (W_{jy} T_{jy})}{\sum_j W_{jy}}, \quad \text{(Eq. 1)}$$

where T_{ky} is the area-weighted mean temperature in region *k* for year *y*, W_{jy} is the area size for smaller geographic area *j* (within each region *k*) with samples for year *y*, T_{jy} is the mean temperature for geographic area *j* in year *y* which is defined as:

$$T_{jy} = \frac{\sum_i T_{iy}}{n_{jy}}, \quad \text{(Eq. 2)}$$

where T_{iy} is the temperature for station i in year y from geographic area j, n_{jy} is the number of stations sampled in geographic area j in year y.

For the subsurface temperature from the 250-m layer, the BS and AI appear generally warmer since 2014, while the GOA appears relatively warmer since 2017 (Fig. 36). This pattern is different from that observed in satellite-derived sea surface temperatures, indicating some differences in the marine processes at the surface versus at depth (Ferris 2021). Looking at individual stations, the annual trends in regions are captured quite well by the area-weighted sub-regional means (black lines and points), illustrating the aforementioned regional warming in recent years (Fig. 36). The area-weighted mean temperature was very similar to the regional mean temperature when only consistently sampled stations were included for the BS, AI, and the EGOA; these were generally consistent for the CGOA, with the exception of 2007, 2010, 2018, and 2019 (Fig. 36). These latter discrepancies are clearly the result of only having two stations sampled every year from the CGOA, stations 73 and 74 which are two of the three furthest west stations, so these are not considered representative of the entire region and make it important to look at the broader spread of stations. The area-weighted temperatures are recommended for tracking subsurface temperatures from this dataset, as they include all available data in a given year, and are not as spatially limited as the consistently sampled stations. The three regions of the GOA appear connected, where some years the CGOA is more similar to the EGOA (e.g., 2007, 2010, and 2016), while other years the CGOA is more similar to the WGOA (e.g., 2005 and 2015), with recent temperatures hovering around the time series mean in all regions (Fig. 36). Still, recent years across Alaska have remained among the warmest observed in this dataset, and subsurface temperature should continue to be monitored on the AFSC longline survey as this short time series continues to grow. The sablefish management regions shown are used in the sablefish ecosystem and socioeconomic profile (ESP) for sablefish (Goethel et al. 2022), while the ecosystem status reports (ESRs) have slightly different regional boundary definitions (Ferris and Zador 2021, Ortiz and Zador 2021, Siddon, 2021).

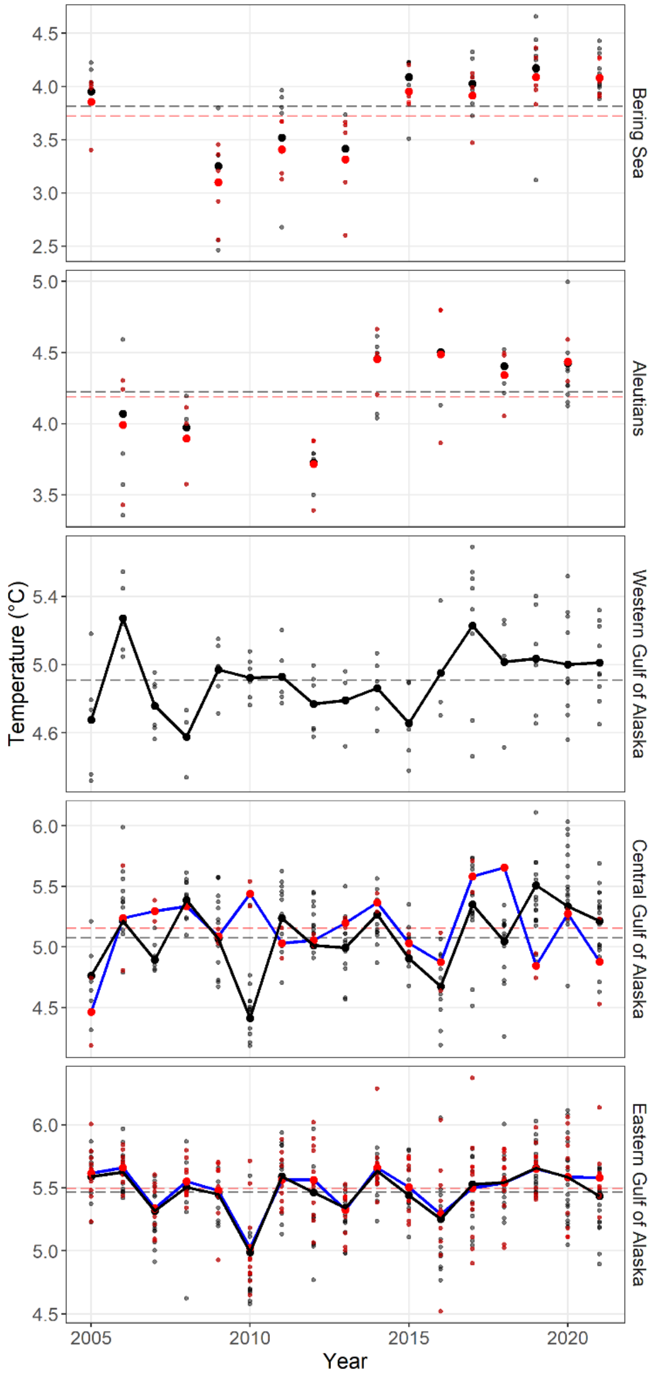

Figure 36. -- Regional trends in subsurface temperature (250 m), with small grey points showing each station and small red points for stations sampled every year. Black points (and lines when time series is contiguous) are regional mean temperatures weighted by area of smaller geographic sub-regions. Larger red points (connected by a blue line when time series was contiguous) for stations sampled every year (note that no stations in the Western Gulf of Alaska were sampled at 250 m every year). Horizontal dashed lines are overall means for area-weighted (black) and consistently sampled (red) means.

ASSIGNING TEMPERATURE BY DEPTH

Bottom temperature is only measured at one depth at a station, but fishing at each station occurs over a broad range of depths (typically between 100 and 1,000 m) making it difficult to determine the influence of bottom temperature on variables such as catch rates or observed lengths. A method for interpolating (or extrapolating) bottom temperature to nearby shallower (or deeper) depths could provide a proxy of the temperature for each skate of fishing gear, which has a known catch per unit effort (CPUE). The 2019, 2020, and 2021 surveys included two TDRs per day (one shallower and one deeper approximately 8 km apart) and allowed for two interesting comparisons: 1) how well a deeper temperature profile can predict a nearby shallower bottom temperature and 2) how well regionally averaged temperature profiles can model temperature to deeper depths (Fig. 37). To infer shallower bottom temperatures from profiles, the shallower bottom temperature was predicted from the nearby deeper profile's midwater temperature at the shallower bottom depth. To infer bottom temperatures occurring deeper than the maximum depth from a profile, the mean temperature by depth of all nearby temperature-depth profiles (in this case, region was defined by fishery management plan subareas) for a given year, excluding the station being considered. In each year and region combination, the deepest bottom depth cannot be directly estimated because the other profiles do not provide any information for that depth, so in these instances, a linear model of the last 100 m by year and region was used to predict the temperature at the deeper bottom depths:

$$T_{zky} = \alpha_{ky} + \beta_{ky} Z_{\mathrm{ky}} + \varepsilon_{zky}, \qquad \text{(Eq. 3)}$$

where T_{zky} is the predicted temperature at depth z, in region k, and in year y, α_{ky} is the estimated intercept for region k and year y, β_{ky} is the estimated slope for region k and year y, Z_{ky} is the bottom depth in region k and year y at which to estimate a temperature, and ε_{zky} is a normally distributed error term.

In general, nearby temperature profiles predicted bottom temperatures well. The midwater temperatures were easily related to nearby bottom temperatures, with reasonable predictions for observed temperatures in 2019, 2020, and 2021, though observations may have been slightly higher (< 0.5 °C) than predictions for warmer temperatures in 2021 (Fig. 38). This suggests that assigning a temperature from a nearby midwater profile to a skate of longline gear fishing on the bottom (and therefore to the catch at that skate) is a reasonable estimate of the actual bottom temperature. Using the regional mean temperature profiles to extrapolate to deeper depths, including extending deeper than any sample in that region using the deepest 100 m to create a linear model, is also a reasonable surrogate for missing temperature data (Fig. 39), particularly because there is much less variability in regional bottom temperature with increasing depth. Combined, these methods can be used to assign temperatures to each skate, allowing analyses of longline survey catch (and length) data with respect to approximate bottom temperatures.

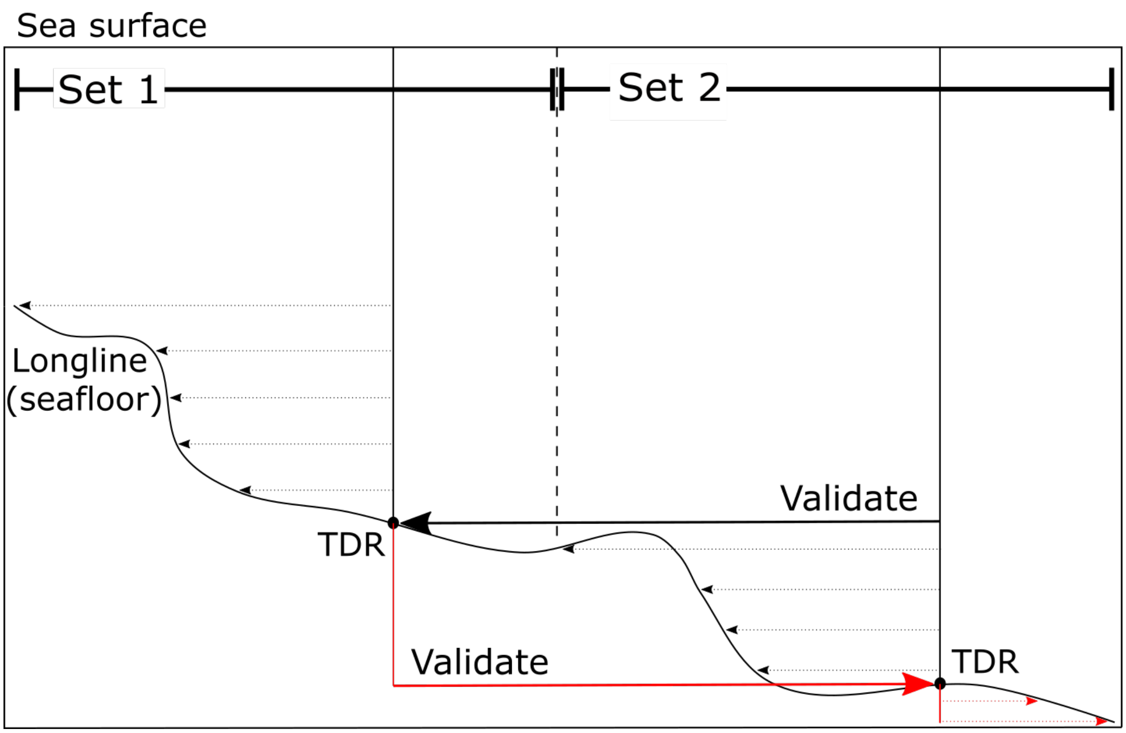

Figure 37. -- A schematic of a typical two set day of fishing with a temperature and depth recorder (TDR) attached on each set, where fishing gear temperatures at shallower bottom depths can be inferred from nearby midwater temperatures (black dotted lines with arrows), and fishing gear temperatures at deeper depths can be inferred from annual FMP subarea means (red dotted lines with arrows). Extrapolation to deeper depths should be limited to instances when the temperature change is linearly predictable, which is often the case in deep water. Bottom temperatures are validated for shallower depths using nearby midwater temperature/depth (solid black line and arrow) and for deeper depths using regional means (and in the deepest cases, linear extrapolation) of temperature at depth (solid red line and arrow).

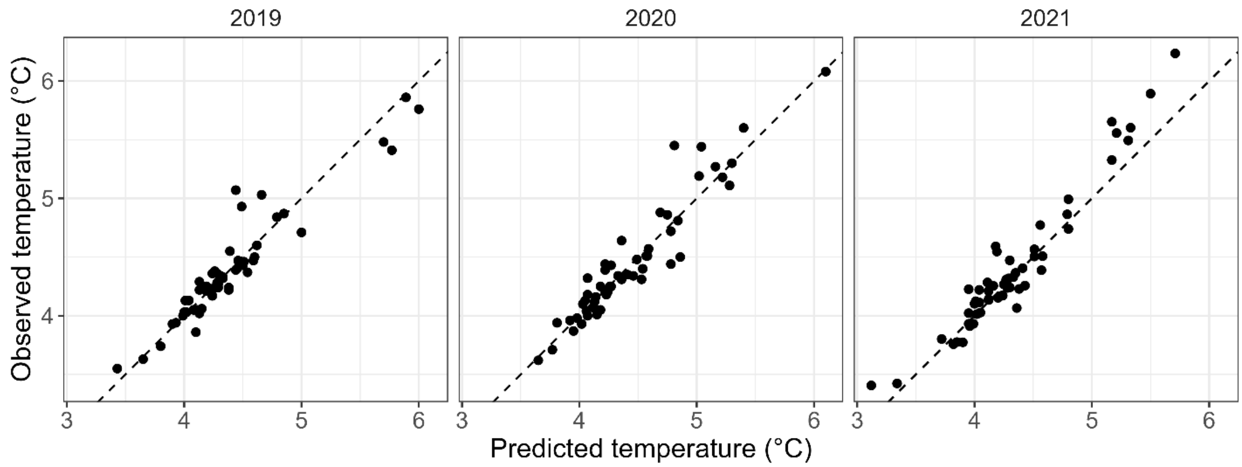

Figure 38. -- A comparison of shallower bottom temperatures (Observed) with nearby midwater temperatures (Predicted), where the dashed line has a slope of 1 and y-intercept of 0.

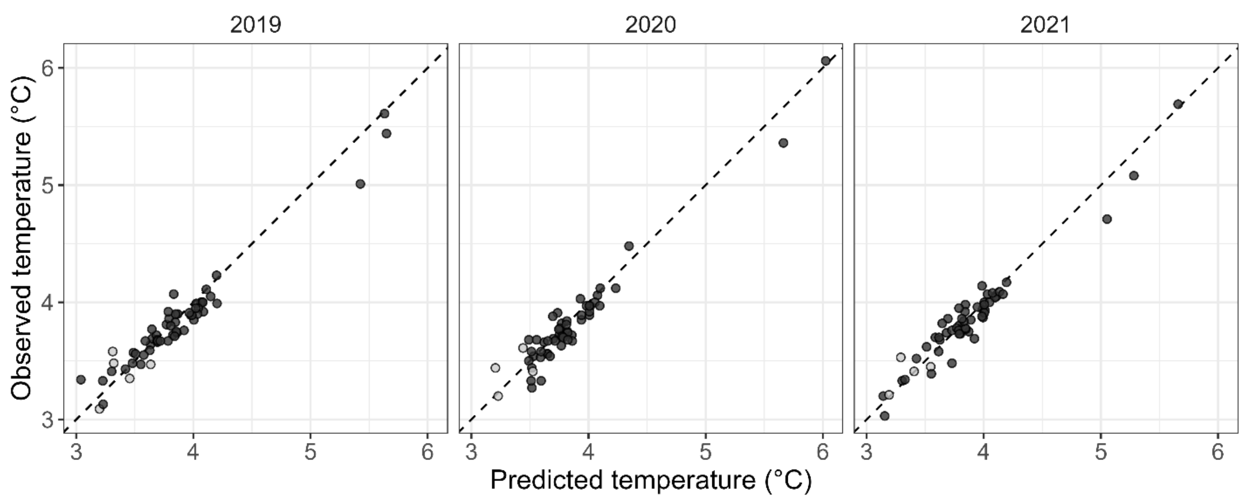

Figure 39. -- A comparison of deeper bottom temperatures (Observed) with regionally predicted temperatures (dark grey) and linearly predicted for the deepest bottom temperatures in each region (light grey), where the dashed line has a slope of 1 and y-intercept of 0.

TEMPERATURE INVERSION LAYERS

Water temperature generally decreases with increasing depth, but a temperature inversion layer (TIL) exists when water temperature increases with increasing depth. This feature is common in the North Pacific Ocean and is believed to be related to currents and mixing of water masses (Ueno and Yasuda 2005). In order to identify a TIL, the following steps were carried out on each successful downcast: 1) interpolated temperatures from 1-m increments deeper than 20 m were used to avoid including a TIL associated with the surface layer, 2) a moving-window average with a span of 5 m was calculated to smooth the profile, 3) a matrix (lower triangle used) of the temperature difference between each of the moving-window averages was created, 4) the greatest temperature increase was identified, and 5) only temperature increases of > 0.1 °C with a depth change of 10+ m was included. On occasion, the identified deep bound of a TIL was the deepest temperature from a profile, indicating that the entire TIL was not entirely captured and suggesting that the TIL could have extended over a greater depth and temperature if a deeper profile had been conducted. This method is similar to those used by Ueno and Yasuda (2005), but the regions covered by the survey typically had TILs occurring at depths between 200 m and 300 m, so we did not exclude profiles shallower than 500 m as they had done.

Identified TILs were used to further characterize subsurface water temperatures from each station, region, and year. At each station with a TIL, the minimum and maximum temperatures with the associated minimum and maximum depths were extracted, and used to determine the change in temperature ΔT and the change in depth ΔZ (Fig. 40). An annual percentage of stations with a TIL was determined for each year and region by dividing the number of stations with a TIL by the number of stations with a TDR downcast.

Of the 1,329 temperature profiles, 721 had a TIL present below 20-m depth that occurred over 10 m and increased in temperature by at least 0.1 °C. The magnitude of the thickness of the TIL and the change in temperature that occurred varied by region and year, with the WGOA exhibiting the greatest in both, and the EGOA exhibiting the least in both (Fig. 41). During the heatwave in the GOA from 2014 to 2016, and again in 2019, there were fewer and smaller TILs (Fig. 42). The lack of TILs in the GOA during the heatwave, especially 2015, 2016, and 2019, is evident, though both 2020 and 2021 appear to have larger TILs suggesting that these features are sensitive to annual surface temperature fluxes (Figs. 42 and 43). The greatest difficulty is addressing temperature-depth profiles that do not sample deep enough to fully capture TILs. This discrepancy is particularly obvious in deeper stations (set two) starting in 2019 that identified more TILs than the shallower station and identified larger temperature (and depth) changes, though the deeper sets generally provide the same message as the shallower sets (Figs. 41–43).

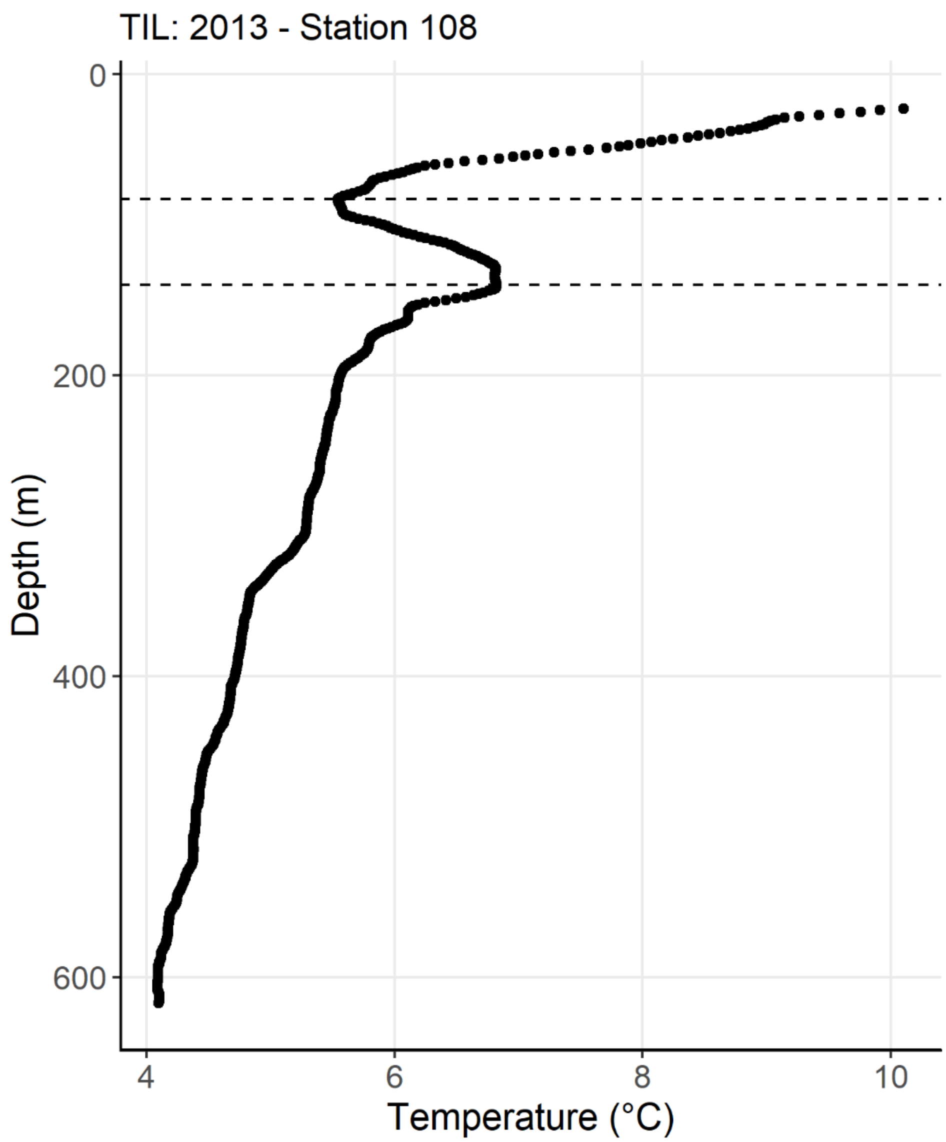

Figure 40. -- An example of a temperature inversion layer (TIL) identified from a temperature-depth profile of station 108 in 2013. In this example, the beginning and end of the TIL is indicated by the two dashed horizontal lines.

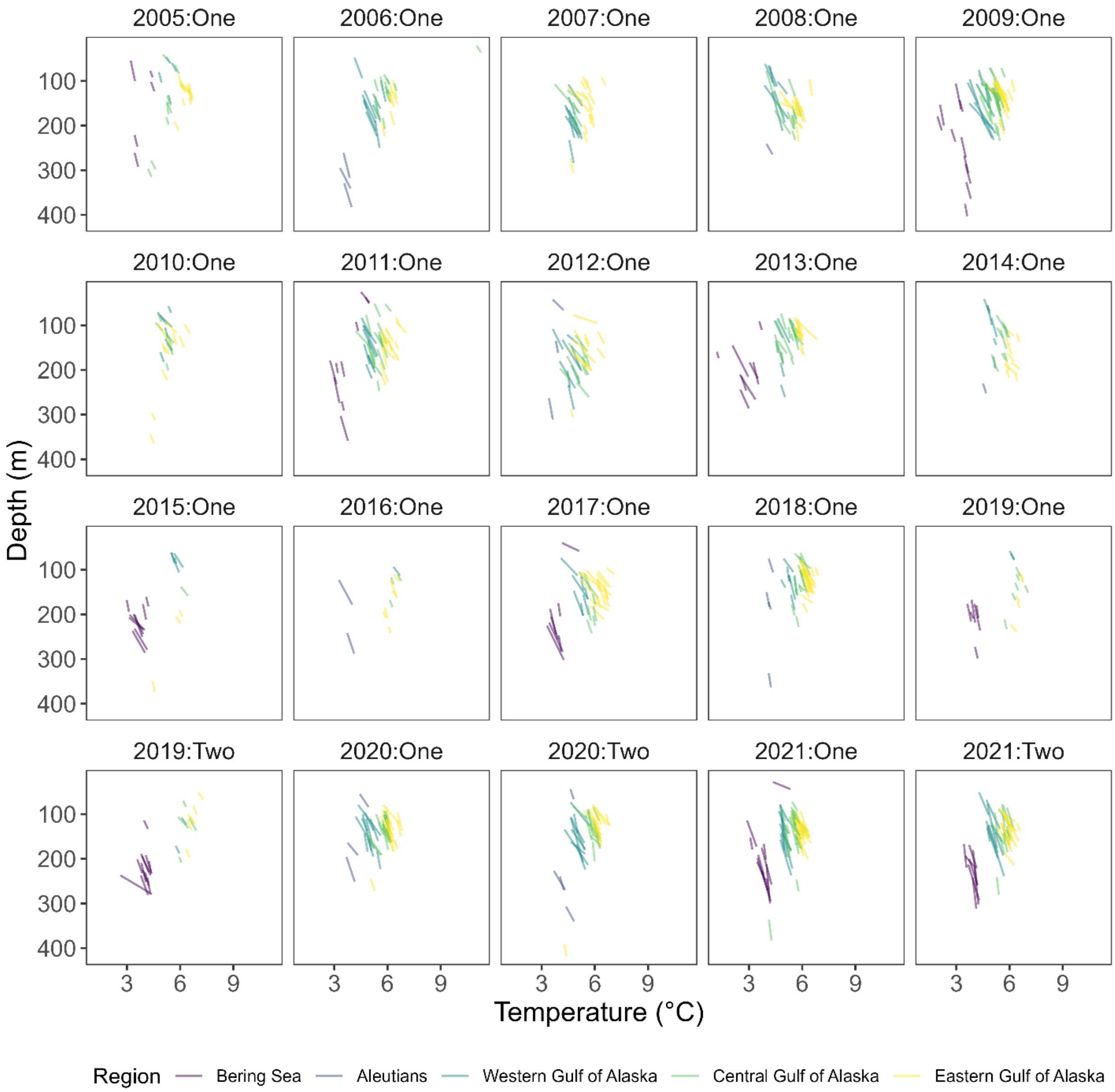

Figure 41. -- An illustration of identified temperature inversion layers (TIL), with each line indicating the change in temperature and depth for a TIL at a station by year:set combination (panel) and region (color). For 2019 through 2021, there are two panels because of the addition of deeper profiles conducted on the second set of each station.

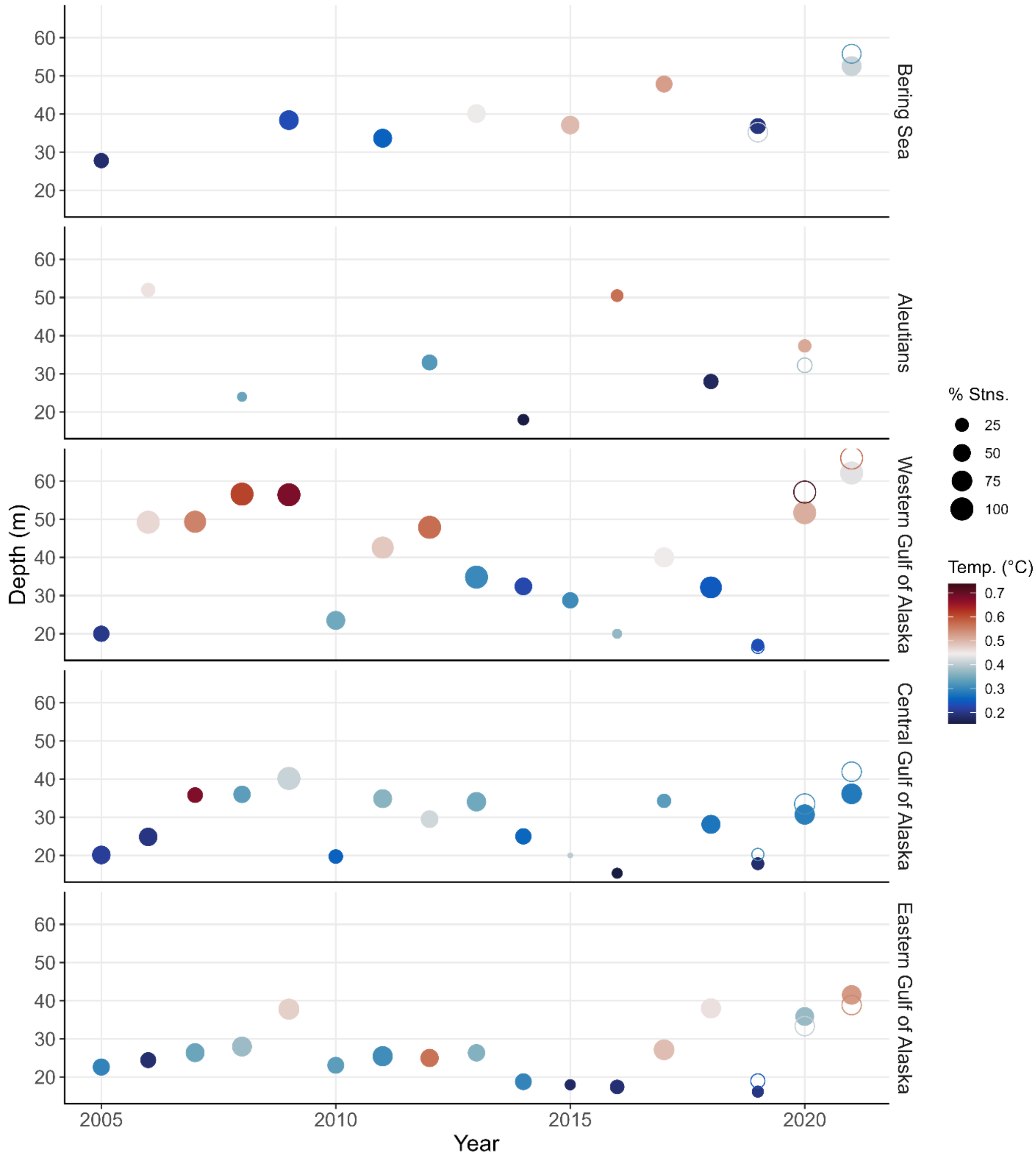

Figure 42. -- A time series illustrating the mean change in depth (y-axis), mean change in temperature ("Temp. (°C)" on the color scale), and percent of stations with an identified temperature inversion layer by region ("% Stns." indicated by the size). Open circles for 2019 to 2021 are from deeper profiles conducted on the second set of survey stations and treated separate from profiles on the first set.

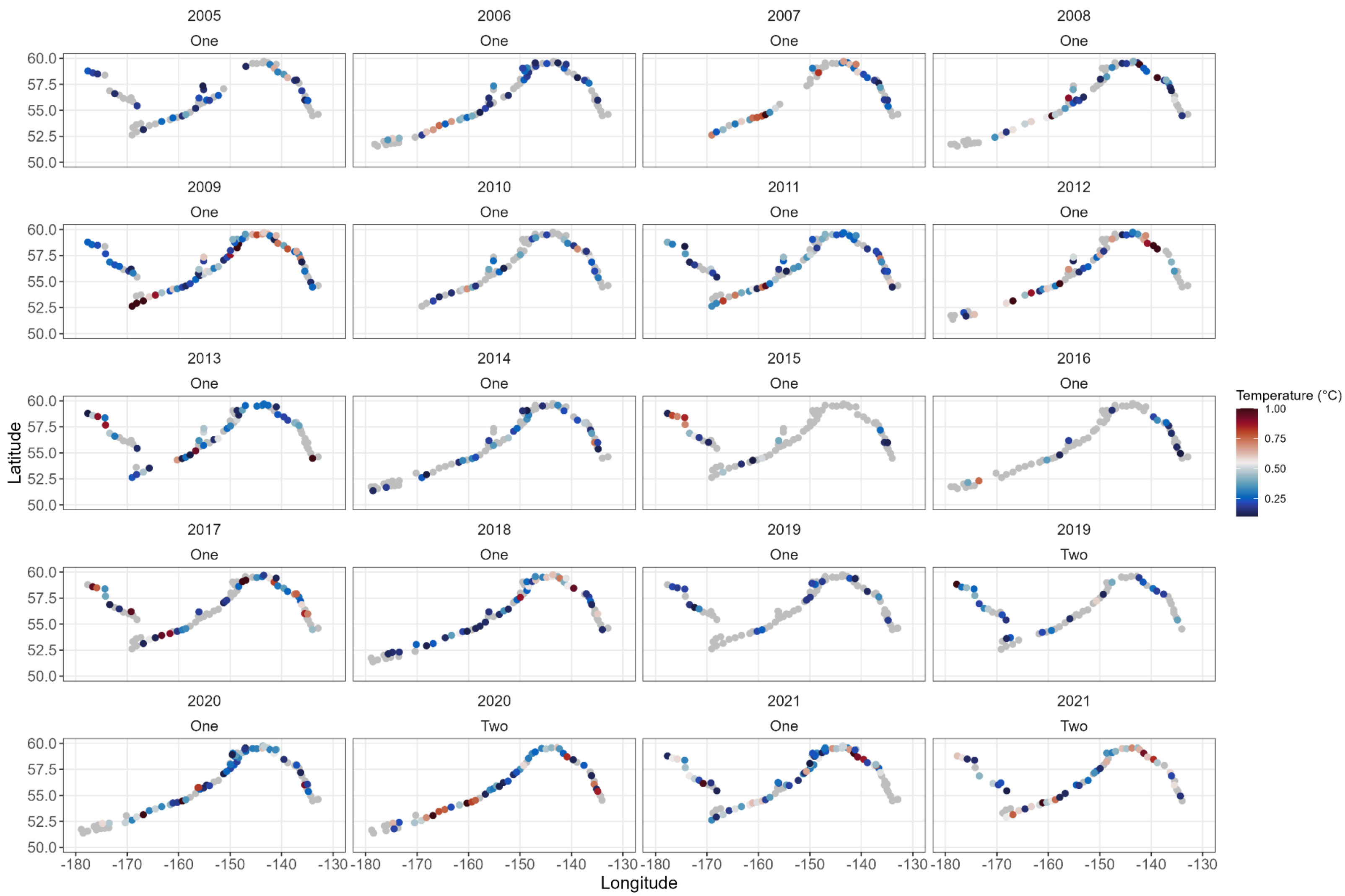

Figure 43. -- Spatial display of the identified change in temperature for temperature inversion layers (TIL), where grey indicates that no TIL was identified. Set "One" is shown for every year, and 2019 through 2021 also include a second plot from the deeper set "Two". Temperature changes that were >1°C were set to 1°C for visualization purposes.

TIDES

One advantage to having the TDR record data at a single point for several hours, is that a stationary measure of pressure will record changing pressure associated with tidal fluxes. As the TDR records pressure (depth) every ten seconds, gradual increases, decreases, or transitions (e.g., flooding tide reaches slack high tide, then starts to ebb), may be detected. An algorithm to filter out noise from setting and hauling was used. In order to estimate the stage of the tide from the TDR, a cosine equation for a simplified tide cycle that occurs every 12 hours and 25 minutes, was used:

$$y_t = \hat{a} * \cos\big(k * (t - \hat{p})\big) + \hat{q} + \varepsilon, \quad \text{(Eq. 4)}$$

where $\hat{a}$ is the estimated amplitude:

$$\hat{a} = \frac{(\widehat{Z_{max}} - \widehat{Z_{min}})}{2}, \quad \text{(Eq. 5)}$$

which is derived from the estimated maximum depth $\widehat{Z_{max}}$ (i.e., depth at high tide) and the estimated minimum depth $\widehat{Z_{min}}$ (i.e., depth at low tide). The estimated mean depth $\hat{q}$ is:

$$\hat{q} = \frac{(\widehat{Z_{max}} + \widehat{Z_{min}})}{2}, \quad \text{(Eq. 6)}$$

k is the constant period in radians assumed to be equal to 12 hours and 25 minutes (12.4167):

$$k = \frac{2\pi}{12.4167}, \quad \text{(Eq. 7)}$$

$\hat{p}$ is the estimated phase shift (i.e., the time at which the high tide occurs), y_t is the recorded depth at time t, and ε is the error term:

$$\varepsilon \sim N(0, \hat{\sigma}^2). \quad \text{(Eq. 8)}$$

The parameters $\widehat{Z_{max}}$, $\widehat{Z_{min}}$, $\hat{p}$, and $\hat{\sigma}$ were estimated by maximum likelihood estimation for each TDR deployment via minimizing the negative log-likelihood. To assess how the model behaves and provide good estimates of starting values, depth observations were simulated for 2.5 hours (10-second intervals) for tides with a Z_{max} = 555 m, Z_{min} = 553.5 m, and phase shift (p) of 1, 3, 5, 7, 9, 11, 13, and 15 hours. Code and results of this simulation are shown (Appendix).

The model provided parameter estimates for all TDR casts, but preliminary examination of plots showed that there were occasionally poor fits to the data. Therefore, results were filtered to remove TDR casts where $\hat{\sigma} > 0.0002$ and $0.2 < \hat{a} < 10$. In total, tide was discernible in 1,101 casts, which includes casts from the first and second set of the same station (since 2019). There were 115 stations with a discernible tide from the first and second set after filter, and estimates of tidal amplitude and time of the first high tide were generally very similar for these nearby casts (Fig. 44).

This information can be used to assess whether the tide impacts catch per unit effort on the longline survey. When a station includes a slack tide (i.e., at high or low tide), the lack of tidal currents may impact CPUE. Directional tidal currents may create a scent plume from the bait that targets a more or less advantageous fishing area. Additionally, larger or smaller tides may impact the magnitude of tidal currents. In the future, tidal information could be considered to explain variability in catches during the survey. Another use of this method is in geolocation of electronically tagged stationary fish, as pressure measurements from the tag could similarly be used to detect tides which could aid in identifying the location of the fish while at liberty.

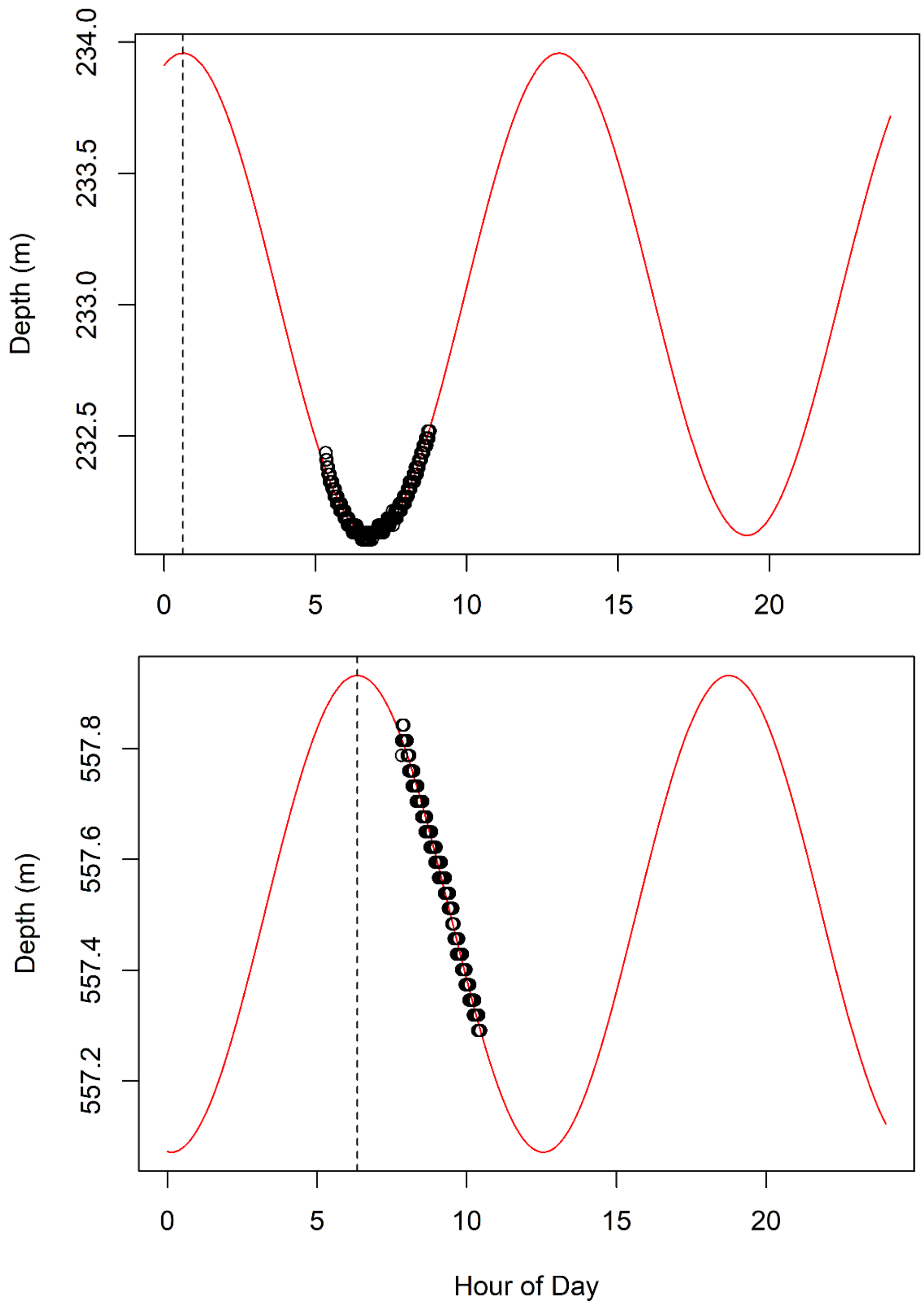

Figure 44. -- Examples of estimating amplitude and timing of the tide, where black points are the depth (converted from pressure) measured by the temperature and depth recorder, and the red line is the maximum likelihood estimated tidal cycle with the timing of the first high tide indicated by the vertical dashed line. The top panel shows station 122 from 2005 capturing a slack low tide, and the bottom panel shows station 18 from 2013 capturing an ebbing tide through the maximum tidal current.

ASSESSING BIAS IN ASSIGNED DEPTH

The mean bottom depth from the TDR was compared to the recorded (or interpolated) depth from the biologists on the survey. To test for a significant difference between biologist-assigned depth and TDR-recorded depth, a paired t-test compared each station-year combination. Potential bias was assessed by first detecting whether the mean difference significantly differed from zero. The percent of skates assigned to the incorrect depth strata (deeper or shallower) was also used to assess whether differences impact the survey design and goals.

Biologist-assigned depth was not significantly different than the TDR depth for the 1,356 paired samples which included the deeper sets from 2019 through 2021, with a 95% confidence interval of the mean difference between -1.8 and 1.3 m ($t = -0.35$, $df = 1,355$, and p-value = 0.73) (Fig. 45). Overall, 10.5% of skates were assigned an incorrect depth stratum compared to the TDR recorded depth, but these were split evenly with 5.2% assigned greater than and 5.4% assigned less than the depth recorded by the TDR (Fig. 46). At the extremes, biologist-assigned depth was 177.4 m greater than and 203.5 m less than the TDR-recorded depth. Large discrepancies are likely related to steep slopes when the vessel is not directly over the gear or possible misidentified skate numbers that would result in incorrect pairing. Recent changes to TDR data collection should minimize the potential for these errors in the future. This assessment provides evidence of some misidentification of depths and depth strata but overall confidence that there is little bias in this survey method.

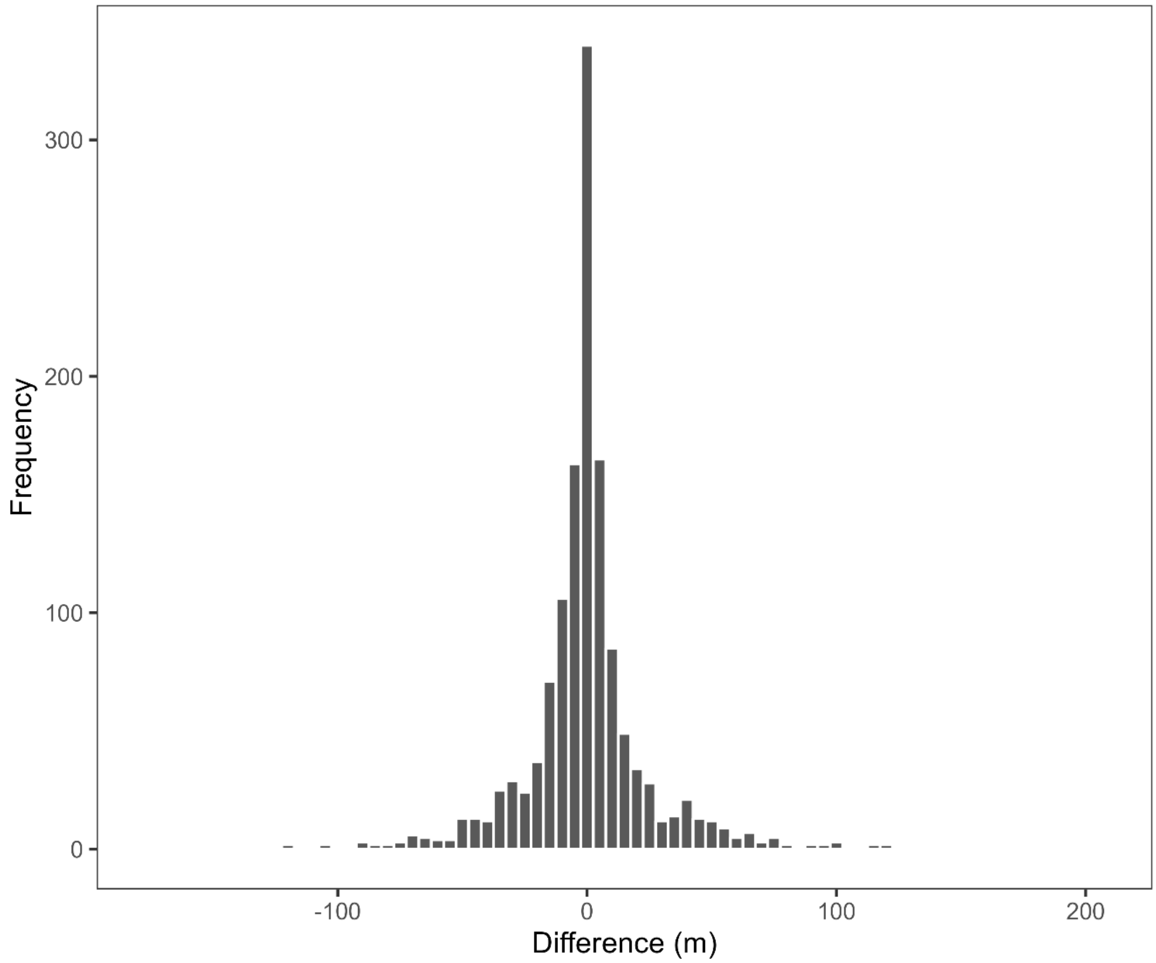

Figure 45. -- Histogram of the difference between TDR depth and biologist recorded depth with 5-m depth bins.

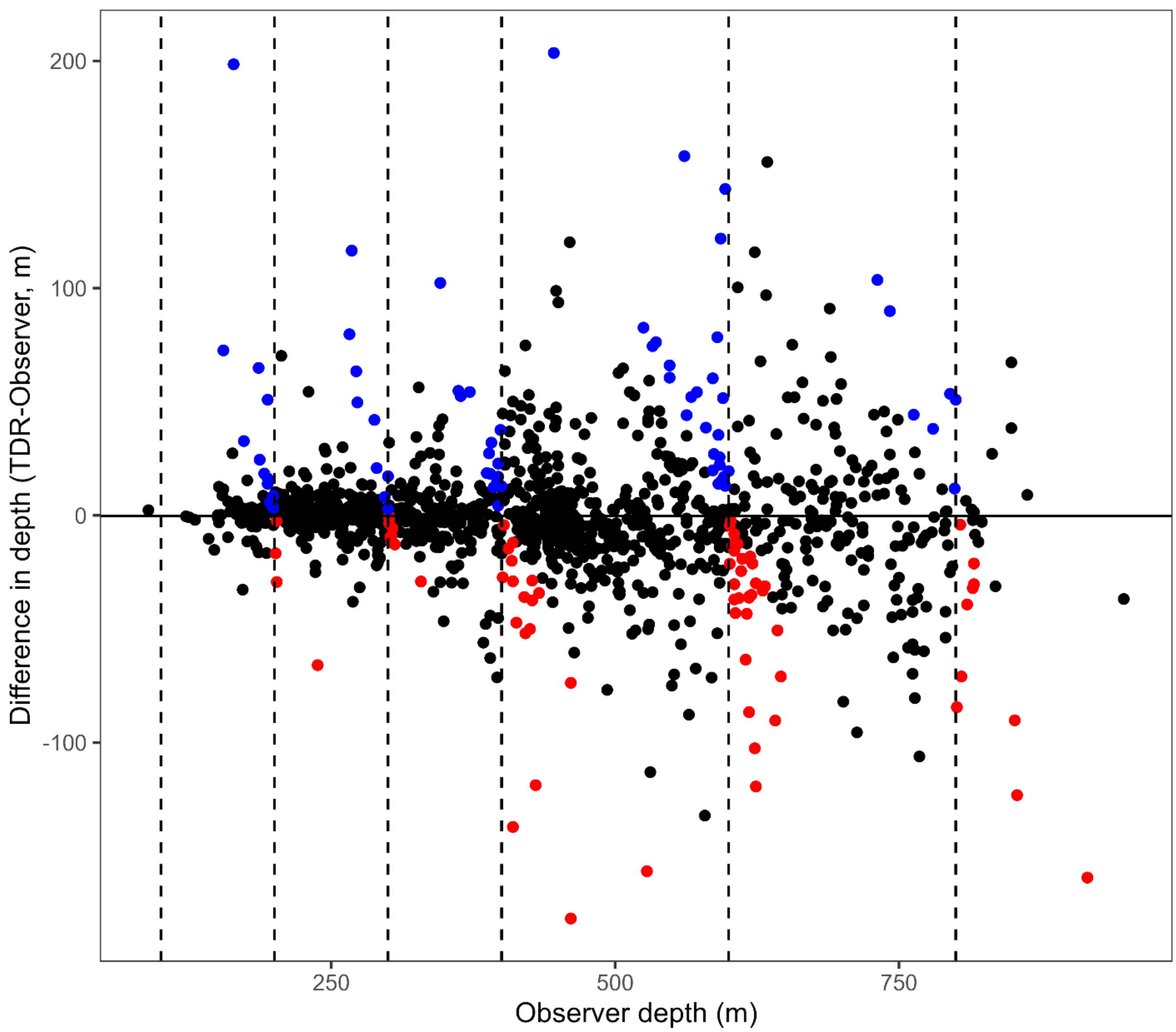

Figure 46. -- The difference between TDR depth and biologist observed ('Observer') depth in meters shown in relation to the biologist observed depth which is used for stratifying catch and length data. Dashed vertical lines indicate the separation of depth strata used on the longline survey, solid horizontal line is the mean difference, red circles indicate that the depth strata was assigned too deep (i.e., the TDR depth would have changed that skate to a shallower depth stratum), and blue circles indicate that the depth strata was assigned too shallow (i.e., the TDR would have changed that skate to a deeper depth stratum).

CONCLUSIONS

It is valuable for the annual AFSC longline survey to record accurate temperature at depth during their operations, as this information has detected changes in subsurface temperature that have occurred since these measurements began. The complexities of utilizing bottom temperature alone from this survey have been discussed, and the relationship between bottom temperatures and nearby midwater temperatures provide regional snapshots of the subsurface thermal environment and insights into potential regional subsurface dynamics. Over time, this dataset can be used to assess long-term trends in subsurface temperature. Beginning in 2021, this environmental data has been synthesized into ecosystem status reports for the Gulf of Alaska, Aleutian Islands, and eastern Bering Sea (Ferris and Zador 2021, Ortiz and Zador 2021, Siddon 2021). A method for interpolating (and extrapolating) bottom temperatures to each skate of gear has been shown, and while other methods may be more appropriate, this exercise has provided an avenue towards examining raw catch in relation to temperature (estimated for the bottom) for the AFSC longline survey. This dataset has been used to propose a method for identifying temperature inversion layers, with the size of the inversion layer and magnitude of the temperature difference relating to overall warmer and cooler subsurface temperatures. These physical features in the water column should be further investigated as a potential mechanism for changes in subsurface temperature to impact egg and larval development and vertical transport. Pressure measurements (measuring depth) were useful in estimating tidal stage during survey fishing and providing evidence that depths (and depth strata) were being appropriately estimated with little bias.

ACKNOWLEDGMENTS

I would like to thank all those in the Alaska Fisheries Science Center Auke Bay Laboratory (ABL) Division's Marine Ecology and Stock Assessment (MESA) group who collected the longline survey data. Thanks to Ivonne Ortiz, Pat Malecha, and Chris Lunsford for their suggestions to improve this document.

CITATIONS

Buckley, T. W., A. Greig, and J. L. Boldt. 2009. Describing summer pelagic habitat over the continental shelf in the eastern Bering Sea, 1982–2006. U.S. Dep. Commer., NOAA Tech. Memo. NMFS-AFSC-196, 49 p.

Cheung, W. W. L., R. Watson, and D. Pauly. 2013. Signature of ocean warming in global fisheries catch. Nature 497:365–368.

Echave, K., C. Rodgveller, and S. K. Shotwell. 2013. Calculation of the geographic area sizes used to create population indices for the Alaska Fisheries Science Center longline survey. U.S. Dep. Commer., NOAA Tech. Memo. NMFS-AFSC-253, 93 p.

Ferriss, B. E., and S. Zador. 2021. Ecosystem Status Report 2021: Gulf of Alaska, Stock Assessment and Fishery Evaluation Report, North Pacific Fishery Management Council, 1007 West Third, Suite 400, Anchorage, AK 99501.

Goethel, D. R., D. H. Hanselman, C. J. Rodgveller, K. B. Echave, B. C. Williams, S. K. Shotwell, J. Y. Sullivan, P. F. Hulson, P. W. Malecha, K. A. Siwicke, and C. R. Lunsford. 2021. Assessment of the sablefish stock in Alaska, in: Stock assessment and fishery evaluation report for the groundfish resources of the GOA and BS/AI. North Pacific Fishery Management Council, 605 W 4th Ave., Suite 306 Anchorage, AK 99501, USA.

Kearney, K., A. Hermann, W. Cheng, I. Ortiz, and K. Aydin. 2020. A coupled pelagic–benthic–sympagic biogeochemical model for the Bering Sea: documentation and validation of the BESTNPZ model (v2019. 08.23) within a high-resolution regional ocean model. Geoscientific Model Development 13:597–650.

Kotwicki, S., and R. R. Lauth. 2013. Detecting temporal trends and environmentally-driven changes in the spatial distribution of bottom fishes and crabs on the eastern Bering Sea shelf. Deep Sea Res. Pt. II: Top. Stud. Oceanogr. 94:231–243.

Krieger, J. R., A. H. Beaudreau, R. A. Heintz, and M. W. Callahan. 2020. Growth of young-of-year sablefish (*Anoplopoma fimbria*) in response to temperature and prey quality: Insights from a life stage specific bioenergetics model. J. Exp. Mar. Biol. Ecol. 526:151340.

Laurel, B. J., and L. A. Rogers. 2020. Loss of spawning habitat and prerecruits of Pacific cod during a Gulf of Alaska heatwave. Can. J. Fish. Aquat. Sci. 77:644–650.

Lauth, R. R., E. J. Dawson, and J. Conner. 2019. Results of the 2017 eastern and northern Bering Sea continental shelf bottom trawl survey of groundfsh and invertebrate fauna. U.S. Dep. Commer., NOAA Tech. Memo. NMFS-AFSC-396, 260 p.

Locarnini, R. A., A. V. Mishonov, O. K. Baranova, T. P. Boyer, M. M. Zweng, H. E. Garcia, J. R. Reagan, D. Seidov, K. W. Weathers, C. R. Paver, and I. V. Smolyar. 2019. World Ocean Atlas 2018, Volume 1: Temperature. A. Mishonov, Technical Editor. NOAA Atlas NESDIS 81, 52 p.

Meehl, G., A. Hu, B. Santer, and S. Xi. 2016. Contribution of the Interdecadal Pacific Oscillation to twentieth-century global surface temperature trends. Nat. Clim. Change 6:1005–1008.

Mueter, F. J., and M. A. Litzow. 2008. Sea ice retreat alters the biogeography of the Bering Sea continental shelf. Ecol. Appl. 8:309–320.

Nieves, V., J. K. Willis, and W. C. Patzert. 2015. Recent hiatus caused by decadal shift in Indo-Pacific heating. Science 349:532–535.

Ortiz, I., and S. Zador. 2021. Ecosystem Status Report 2021: Aleutian Islands, Stock Assessment and Fishery Evaluation Report, North Pacific Fishery Management Council, 1007 West Third, Suite 400, Anchorage, Alaska 99501.

Reiniger, R. F. and C. K. Ross. 1968. A method of interpolation with application to oceanographic data. Deep Sea Res. 15:185–193.

Rooney, S., C. N. Rooper, E. Laman, K. Turner, D. Cooper, and M. Zimmermann. 2018. Model-based essential fish habitat definitions for Gulf of Alaska groundfish species. U.S. Dep. Commer., NOAA Tech. Memo. NMFS-AFSC-373, 370 p.

Siddon, E. 2021. Ecosystem Status Report 2021: Eastern Bering Sea, Stock Assessment and Fishery Evaluation Report, North Pacific Fishery Management Council, 1007 West Third, Suite 400, Anchorage, Alaska 99501.

Siwicke, K., P. Malecha, and C. Rodgveller. 2022. The 2021 longline survey of the Gulf of Alaska and eastern Bering Sea on the FV *Alaskan Leader*: Cruise Report AL-21-01. AFSC Processed Rep. 2022-01, 27 p. Auke Bay Laboratories, Alaska Fish. Sci. Cent., NOAA, Natl. Mar. Fish. Serv., 17109 Point Lena Loop Road Juneau, AK 99801.

Stevenson, D. E., and R. R. Lauth. 2019. Bottom trawl surveys in the northern Bering Sea indicate recent shifts in the distribution of marine species. Polar Biol. 42:407–421.

Thorson, J.T. 2019. Measuring the impact of oceanographic indices on species distribution shifts: The spatially varying effect of cold-pool extent in the eastern Bering Sea. Limnol. Oceanogr. 64:2632–2645.

Ueno, H., and I. Yasuda. 2005. Temperature Inversions in the Subarctic North Pacific. J. Phys. Oceanogr. 35:2444–2456.

APPENDIX: TIDE SIMULATION

Tidal data were simulated similar to what is seen on the longline survey to test whether the method used was able to recover reasonable estimates for the 'true' phase and amplitude with noise. The minimum and maximum depth were the same for all simulations (min = 553.5 m and max = 555.0 m), with different times of the high tide set between 0100 and 1500 at 2-hour increments. Timing of simulated data was between 0730 and 1000 at 10-s intervals, which is similar to the timing of the morning set on the longline survey, and this captured short windows of various tidal stages such as ebbing, flooding, slack high, and slack low (Appendix Fig. 1). In all instances, the minimum and maximum depth were accurately determined, thus the amplitude was recovered, and the phases were also well resolved (Appendix Fig. 2).

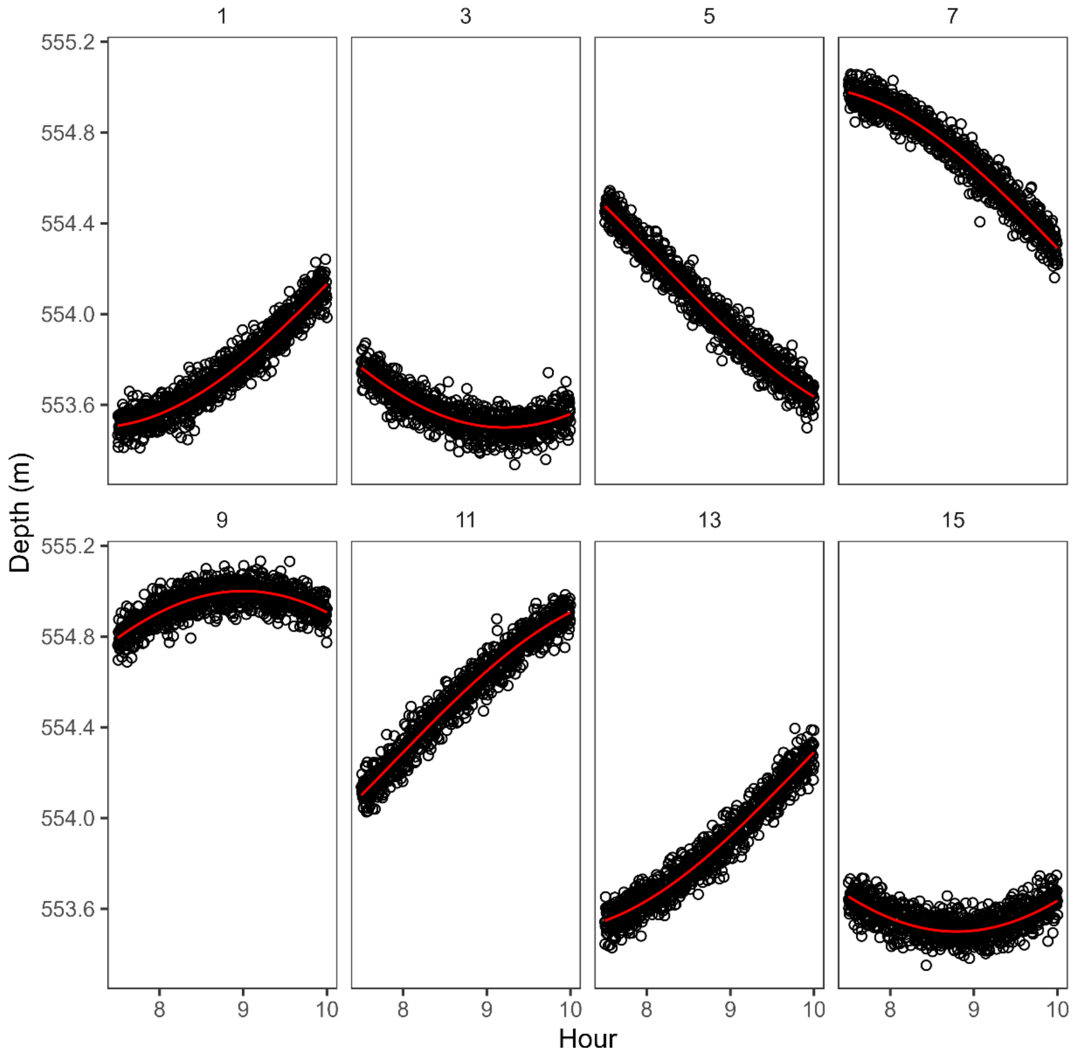

Appendix Figure 1. -- Simulated depth data for tides at various phases (number above each panel), where the red line is the true tidal signal and the black circles are the depth data simulated with error.

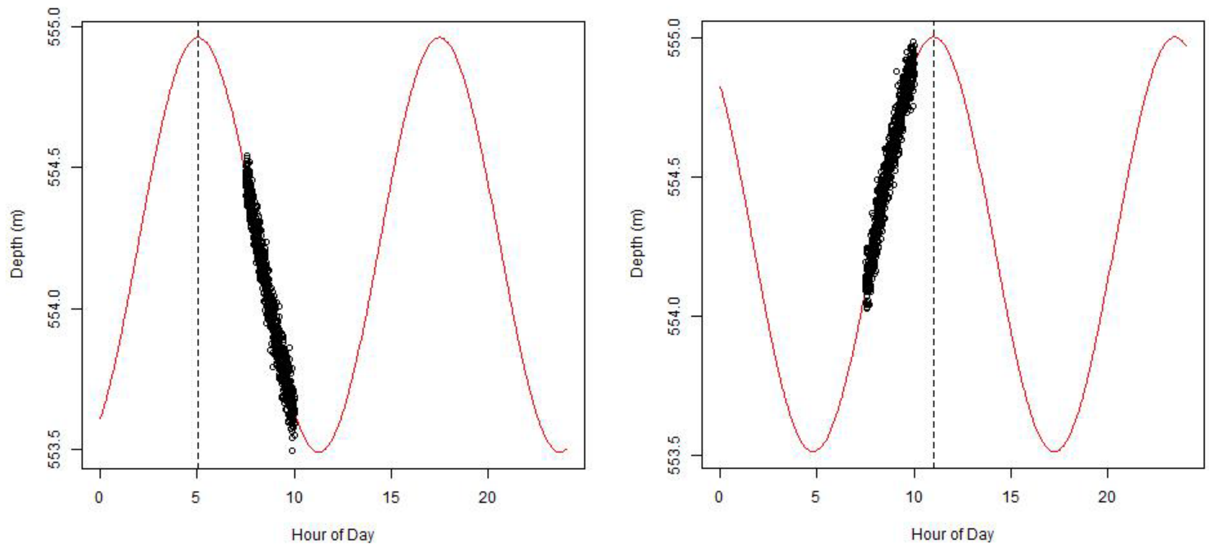

Appendix Figure 2. -- Black points are the simulated depth between 0730 and 1000, and the red line is the maximum likelihood estimated tidal cycle from which the timing and magnitude can be extracted. The left panel shows a high tide simulated at 0500, and the right panel shows a high tide simulated at 1100. Vertical dashed lines are the maximum likelihood estimates of the time of high tide.

R-code for Tide Simulation

```
##############################
#
# Simulate depth data with a tidal signal
# and see how well we can recover the time at high/low tide
#
##############################

# Load packages
library(bbmle)
library(lubridate)
library(tidyverse)

# Set known parameters for the depth at high/low tide
maxZ = 555
minZ = 553.5

k = 2*pi/(12+25/60)  # the period of a tide at 12 hours and 25 minutes
a = (maxZ - minZ) / 2 # amplitude
q = (maxZ + minZ) / 2 # average depth below surface

# Genereate some data similar to a typical TDR set at 10 sec intervals
Hour = rep(seq(7.5,10, by=1/360), 8) # time interval

ps = c(rep(1,901), rep(3,901), rep(5,901), rep(7,901),
       rep(9,901), rep(11,901), rep(13,901), rep(15,901))

Depth = rep(NA, length(Hour))
True = rep(NA, length(Hour))
for( i in 1:length(Hour)) {
  True[i] = a * cos(k*(Hour[i]-ps[i])) + q
  Depth[i] = True[i] + rnorm(1,0,0.05)
}

dat = data.frame(cbind(Hour, Depth, True, ps))

ggplot(dat) +
  geom_point(aes(Hour, Depth), shape=1) +
  geom_line(aes(x=Hour, y=True), color="red") +
  ylab('Depth (m)') +
  facet_wrap(~ps, ncol=4) +
  scale_x_continuous(breaks=c(8,9,10)) +
  theme_bw() +
  theme(panel.grid=element_blank(), strip.background=element_blank())
```

```
# FUNCTIONS FOR ESTIMATING PARAMTERS FOR A COSINE MODEL OF TIDES
# ASSUME A PERIOD OF 12 H AND 25 MIN PER CYCLE
pred_Z = function(maxZ, minZ, p, obs.time) {
  k = 2*pi/(12+25/60)

  a = (maxZ - minZ) / 2 # amplitude
  q = (maxZ + minZ) / 2 # average depth below surface
  y = a * cos(k*(obs.time-p)) + q
  return(y)
}

# A FUNCTION TO PLOT MODELED DATA AGAINST THE OBSERVED DEPTH
plot_tide = function(maxZ, minZ, p, obs.time, obs.Z) {
  pred.Z = pred_Z(maxZ, minZ, p, obs.time=seq(0,24,0.1))
  plot(seq(0,24,0.1), pred.Z, type='l', col="red", #ylim=c(min(obs.Z)-0.2, max(obs.Z)+0.2),
       xlab = "Hour of Day", ylab = "Depth (m)")
  points(obs.time, obs.Z)
  abline(v=p, lty=2)
}

# NEGATIVE LOG-LIKELIHOOD FUNCTION (TO BE MINIMIZED)
nll_fun = function(ln_maxZ, ln_minZ, ln_p, obs.time, obs.Z, ln_sigma) {
  maxZ = exp(ln_maxZ)
  minZ = exp(ln_minZ)
  p = exp(ln_p)
  sigma = exp(ln_sigma)

  pred.Z = pred_Z(maxZ, minZ, p, obs.time)

  logLike = dnorm(x=log(obs.Z), mean=log(pred.Z), sd=sigma, log=TRUE)

  NLL = -1*sum(logLike)

  return(NLL)
}

test = data.frame()
for( p1 in unique(dat$ps)) {
  tdr = dat[dat$ps==p1, ]

  fit.nll  = mle2(nll_fun, start = list(ln_maxZ=log(max(tdr$Depth)),
           ln_minZ=log(min(tdr$Depth)),
                              ln_p=log(mean(tdr[ tdr$Depth==max(tdr$Depth), "Hour"])),
                              ln_sigma=log(0.5)),
              data=list(obs.Z=tdr$Depth, obs.time=tdr$Hour),
              method="Nelder-Mead", optimizer="nlminb",
```

```
              control=list(maxit=1e6))

  maxZ = exp(coef(fit.nll)[1])
  minZ = exp(coef(fit.nll)[2])
  p = exp(coef(fit.nll)[3])
  sigma = exp(coef(fit.nll)[4])

  if(maxZ<minZ) {
    maxZ = exp(coef(fit.nll)[2])
    minZ = exp(coef(fit.nll)[1])
    p = exp(coef(fit.nll)[3]) + 6.208333
  }

  tide = c(p1, maxZ, minZ, p, sigma)
  test = rbind(test, tide)

  jpeg(file=paste0("p_",p1,".jpg", sep=""))
  plot_tide(maxZ=maxZ, minZ=minZ, p=p, obs.time=tdr$Hour, obs.Z=tdr$Depth)
  dev.off()
}

names(test) = c("True.p", "maxZ", "minZ", "est.p", "sigma")
test
test$est.p = ifelse(test$est.p > 12.41667, (test$est.p - 12.41667), test$est.p)

plot(test$True.p, test$est.p)
par(mfrow=c(1,3))
hist(test$maxZ)
hist(test$minZ)
hist(test$sigma)
```

U.S. Secretary of Commerce
Gina M. Raimondo

Under Secretary of Commerce for Oceans and Atmosphere
Dr. Richard W. Spinrad

Assistant Administrator, National Marine Fisheries Service. Also serving as Acting Assistant Secretary of Commerce for Oceans and Atmosphere, and Deputy NOAA Administrator
Janet Coit

May 2022

www.nmfs.noaa.gov

OFFICIAL BUSINESS

National Marine Fisheries Service
Alaska Fisheries Science Center
7600 Sand Point Way N.E.
Seattle, WA 98115-6349